Surface Properties and Antioxidant Activity of Silicate and Borosilicate Bioactive Glasses

**Surface properties and antioxidant activity of silicate and borosilicate bioactive glasses**

S. Ferraris[1], I. Corazzari[2], F. Turci[2], A. Cochis[3], L. Rimondini[3], S. Spriano[1], J. Massera[4], E. Vernè[1]

[1] Department of Applied Science and Technology, Institute of Materials Physics and Engineering, Politecnico di Torino, Torino, Italy

[2] Department of Chemistry and "G. Scansetti" Interdepartmental Center for Studies on Asbestos and Other Toxic Particulates, University of Torino, Torino, Italy

[3] Department of Health Sciences, Center for Translational Research on Autoimmune and Allergic Diseases–CAAD, University of Piemonte Orientale UPO, Novara, Italy

[4] Faculty of Medicine and Health Technology, Laboratory of Biomaterials and Tissue Engineering, Korkeakoulunkatu 3, 33720, Tampere University, Tampere, Finland

**Corresponding Author**

Sara Ferraris

sara.ferraris@polito.it

**Abstract**

In this work, silicate and borosilicate bioactive glasses have been synthetized and characterized. The antioxidant activity, in presence and absence of human osteoblasts' progenitor cells, of the different glass compositions has been correlated to the surface properties: wettability, zeta potential, hydroxylation degree, reactivity in SBF and Tris buffer. An enhancing effect of boron in the glass reactivity and a stabilizing role of Sr and Mg was evidenced. The scavenging potential of the analyzed bioactive glasses towards reactive oxygen species (ROS) was clearly proved. Moreover, cellular tests confirmed the protective effect of the bioactive glasses towards viable cells acting as ROS/RNS species scavenger. The obtained results represent an original improvement of the knowledge concerning the intrinsic antioxidant ability of bioactive glasses with different compositions and the mechanisms involved in.

**Keywords: Glass; Surfaces; Chemical properties; Biomedical applications; Antioxidant activity**

## 1. Introduction

Bioactive glasses are a class of biomaterials widely studied and applied in several field of tissue engineering, mainly in bone tissue surgery [1]. Their bioactivity mechanism is well known and reported in literature, as a sequence of reactions that occurs *in vitro* by soaking in solutions with a composition analogous to the inorganic part of human plasma (Simulated Body Fluid -SBF): it starts with a fast ions exchange at the glass/solution interface, between the alkaline ions released by the glass surface and the hydrogen ions in the solution, followed by the formation of free Si-OH groups (silanols) and subsequent polycondensation to develop a silica gel layer. This step produces a reduction of hydrogen ions in the solution and give rise to a rise in pH, a feature that can be observed not only in SBF, but also in Tris buffer [2]. Silica gel stimulates the diffusion of $Ca^{2+}$ and $PO_4^{3-}$ ions from the fluids and their adsorption and further reaction to form a hydroxyapatite (HAp) layer, similar to the mineral part of the bone [3, 4]. The bioactivity mechanism has been observed both in silica based bioactive glasses and in borosilicate bioactive glasses [1-7], which show high conversion rate to hydroxyapatite [8].

Recently, it was postulated that the formation of HAp is a useful stage for bioactive behavior and bone remodeling, but not the critical one. Key mechanisms seem to be related to the ionic dissolution products from the degrading bioactive glass, including soluble silica and calcium ions during the very early stage of the bioactivity mechanism, as well as a variety of surface properties of the glass itself, such as surface area, roughness, surface charge (zeta potential), chemistry and topography [9]. All these characteristics seem to contribute to the regulation of bone remodeling process in synergy with a variety of biological species, including those responsible for local and systematic stress actions [9]. In particular, the occurrence of oxidative stress, due to an imbalance between the production and the consumption of Reactive Oxygen Species (ROS), can enhance osteoclast activity and lead to bone loss and osteoporosis [9-11]. An increase of the ROS level is often related to several adverse events associated to bone surgery (bone trauma and injuries, inflammation and infection) so the development of biomaterials for bone contact with antioxidant activity represents a very challenging field of investigation.

It was already reported in literature that the composition of bioactive glasses can be easily tailored by doping with trace and therapeutic ions (e.g. Mg, Zn, Sr, Mn, Ag or Cu) with antibacterial, osteogenic or angiogenetic properties [9, 12]. Moreover, bioactive glasses doped with cerium have shown the ability to degrade $H_2O_2$ by a mechanism similar to the catalase enzyme [13, 14]. Furthermore, a bioactive glass doped with strontium revealed the ability of increasing the cellular antioxidant enzymes activity [15, 16] and very recently it was assessed that tellurium-doped glasses possess strong antibacterial and antioxidant effects [17]. Very recently, an intrinsic antioxidant activity of undoped silica based bioactive glasses, associated with their hydroxylation degree, has been reported [18, 19].

In order to extend the knowledge on the correlation between antioxidant activity and bioactive glass chemical properties, in the present work, a set of silicate and borosilicate bioactive glasses have been designed, synthetized and characterized. Differently from the preliminary previous work by the authors [19], which was focused on simple silica-based bioactive glasses constituted by the same oxides in different proportion with consequent different reactivity here the study is extended to various glass compositions, with includes both silicate and borate glasses, with the addition of different oxides which affect the

structure and the reactivity of the glasses. Moreover, a more in-depth investigation of the mechanism beyond bioactive glass antioxidant ability, in acellular and cellular environments, is performed. In particular, the antioxidant activity, in presence and absence of cells, has been investigated and correlated to the surface properties (wettability, zeta potential, hydroxylation degree, reactivity in SBF and Tris buffer) of the various glass compositions, aiming to further understand the mechanisms involved in the intrinsic antioxidant ability of bioactive glasses.

## 2. Materials and methods

### *2.1 Glasses preparation*

Four different glass compositions have been appropriately designed and synthetized, starting from the $SiO_2$-CaO- $Na_2O$ system, progressively modified by the partial substitution of $SiO_2$ and CaO with different network former and modifier oxides respectively, obtaining systems of increased complexity and different glass structure and reactivity (Table 1).

Moving from SCNB, which is a simple silica based bioactive glass containing only silica, calcium oxide and sodium oxide, as in a previous work of the authors [19], the composition has been modified by the addition of phosphorous oxide (1.72 %mol) for B0, B50 and B50Sr10, of boron oxide (partially substituting silica with 26.93 %mol in B50 and B50 Sr10) and of magnesium and strontium oxides (as 5 and 10 %mol) in to B50Sr10. This compositional design is aimed at the investigation of the role of glass composition, structure, reactivity and hydroxylation degree on their antioxidant activity. Moreover, B50Sr10 contains Sr, which is known for its antioxidant activity [15, 16] and borosilicate glasses (B50 and B50Sr10) present an improved sintering ability, useful for the design of antioxidant bioactive scaffolds.

**Table1:** Compositions (%mol oxides) of the investigated bioactive glasses

| **Oxides [%mol]** | **SCNB** | **B0** | **B50** | **B50Sr10** |
|---|---|---|---|---|
| **$SiO_2$** | 55.6 | 53.86 | 26.93 | 26.93 |
| **CaO** | 21.7 | 21.77 | 21.77 | 6.77 |
| **$Na_2O$** | 22.7 | 22.66 | 22.66 | 22.66 |

| | | | | |
|---|---|---|---|---|
| **$P_2O_5$** | - | 1.72 | 1.72 | 1.72 |
| **$B_2O_3$** | - | - | 26.93 | 26.93 |
| **MgO** | - | - | - | 5.0 |
| **SrO** | - | - | - | 10.0 |

The glasses were produced by the traditional melt-quenching technique. The powder precursor oxides (supplied from Sigma Aldrich) were weighed, gently blended and crushed in a ceramic mortar. The obtained batch was transferred in a platinum crucible and melted into a high temperature furnace. The melt was carefully stirred and cast into a preheated graphite mold to produce two cylindrical rods of 10 mm diameter. Finally, the rods were annealed to remove any residual stress. The annealing temperatures were chosen slightly below the glass transition temperatures of the various glasses (Tgs) obtained from Differential Thermal Analyses measurements (DTA, not reported). The processing temperatures (melting of the precursors and annealing temperature), including various intermediate steps (when necessary) are reported in table 2.

**Table 2:** Glasses processing protocols

| Glass | Precursors melting T (°C) | Time (minutes) | Mould T (°C) | Annealing T (°C) | Annealing time (hours) |
|---|---|---|---|---|---|
| SCNB | 1450 | 120 | 300 | 520 | 6 |
| B0 | 1400 | 120 | 300 | 520 | 6 |
| B50 | 600 | 30 | 300 | 450 | 6 |
| | 1000 | 30 | | | |
| | 1250 | 30 | | | |
| B50Sr10 | 600 | 30 | 300 | 450 | 6 |
| | 1000 | 30 | | | |
| | 1250 | 30 | | | |

Borosilicate glasses were melted step-by-step to prevent excessive foaming. Post-annealing, the glasses were cut into 2 mm thick disks by using a low speed circular saw with a diamond coated blade (bulk samples). The disks were hand polished on both sides, using SiC polishing papers up to grit #4000. Part of

the glasses were crushed and milled in a ceramic mortar. The powders were sieved to a particle size < 38 µm (powder samples).

*2.2 Characterization.*

*2.2.1 Density and Molar Volume*

By using a density determination kit (Ohaus), the density of each glass was calculated, weighing first the bulk sample in air ($w_{air}$), and then in pure ethanol ($w_{eth}$); by knowing the density of the ethanol (0.788 ± 2.2%) the glass density was obtained as:

$$\rho_{sample} = \frac{w_{air}}{w_{air} - w_{eth}} \rho_{eth} \quad (1)$$

The molar volume was calculated using the following equation:

$$V_m = \frac{M}{\rho_{sample}} = \frac{glass\ molar\ mass}{glass\ density} \quad (2)$$

Molar volume has been used for the quantification of differences in network packing because, except for SCNB which is P-free, all bioactive glasses with P have been shown to have some sort of phase separation thereby the phosphate units a Q0 units. For the borosilicate not only, the Phosphate network is in Q0 but also the borate and silicate phase are phase separated and the borate structure is rather hard to identify unambiguously (BO3-BO4-Si-O-B).

*2.2.2 pH measurement and mass loss in SBF and Tris*

Simulated body fluid (SBF) was prepared following the protocol elaborated by Kokubo et al. [20, 21], while TRIS solution was made according to the Sigma Aldrich guideline [22]. The reaction/dissolution test was conducted on both bulk and powder samples.

One bulk sample (300 mg mass) or 300 mg of glass powder were placed inside 15 ml plastic tubes, filled with 10 ml of SBF or TRIS. The tubes were covered with a plastic cap. The samples were kept inside a rotating incubator (120 RPM) at 37 °C for 1, 3, 7 and 14 days. At each time point, the pH was measured at 37 ± 0.5 °C. Then, the disks were removed from the solution, cleaned in ethanol, dried in warm air for 1 day inside a closed labelled polystyrene 24-wells plate, and stored in a desiccator to be later analyzed. As far as powder samples are concerned, the tubes were emptied on a filter paper and rinsed with acetone to stop any ongoing reaction. The powders were let dry for 1 day, and stored in a desiccator.

Furthermore, at each time point, 1 ml of the immersion solution was collected and diluted in 9 ml of ultra-pure nitric acid (1M $HNO_3$) and stored in the fridge, to be later analyzed with the ICP-OES. All tests were repeated in triplicate. Each disk/powder sample was weighed before ($m_{ref}$) and after ($m_{test}$) the immersion in the solution, in order to calculate the sample mass loss following the equation (3):

$$\%\ mass\ loss = \frac{(m_{ref} - m_{test})}{m_{ref}}\ 100 \quad (3)$$

*2.2.3 Ion Release in SBF and TRIS: ICP-OES*

The Inductively coupled plasma - optical emission spectrometry (ICP-OES) was used to measure the ion concentration in both SBF and Tris solutions. The ICP-OES analysis was carried out on the 1:10 nitric acid diluted solutions collected after the immersion of both bulk and powder samples in both SBF and Tris (section 2.2.2). The Si, Ca, Na, P, B, Mg and Sr concentrations were determined with a 5110 ICP-OES (Agilent Technologies). Three replicates were measured for each element, and the results (from the triplicate) averaged.

*2.2.4 Fourier Transform Infrared Spectroscopy (FTIR) FTIR-ATR*

The FTIR analysis was carried out on the bulk samples both before and after the immersion in the buffered solutions, to evaluate the change in the materials' surface structure and potential precipitation of a reactive layer. The specimen was analyzed with Fourier transform infra-red (FTIR) Spectrum One FTIR (PerkinElmer, Inc., USA) in attenuated total reflectance (ATR) mode. The IR absorption spectra were recorded within the range 600-4000 $cm^{-1}$, corrected for Fresnel losses and normalized to the absorption band showing the maximum intensity.

*2.2.5 Raman Spectroscopy*

The Raman spectroscopy analysis was executed on 4 base bulk samples, one for each glass composition, not immersed in any buffered solution. The Raman spectrums were recorded using a 532 nm wavelength laser (Cobolt Samba) and measured with a 300 mm spectrograph (Andor Shamrock 303) and a cooled CCD camera for data collection (Andor Newton 940P). All the spectra were recorded within the range 500-1800 $cm^{-1}$ and normalized to the absorption band showing the maximum intensity.

*2.2.6 X-ray Photoelectron Spectroscopy (XPS)*

As well as for the Raman spectroscopy, the XPS analysis was carried out on 4 base bulk samples, one for each glass composition, not immersed in any buffered solution. Polished and washed surfaces were considered for the test since they are the ones considered for the other characterization and can help understanding the role of surface functional groups on glass behavior (mainly antioxidant ability). X-ray Photoelectron Spectroscopy (XPS, PHI 5000 VER-SAPROBE, PHYSICAL ELECTRONICS) was employed for the determination of the surface chemical composition (survey spectra) and the presence of characteristic functional groups. Both survey spectra (0 - 1200 eV) and high-resolution ones (C, O and Si regions) were acquired. The hydroxylation degree was estimated by the ratio between the area of -OH peak and the area of the other oxygen signals, as previously reported by the authors [19]. In order to guarantee the charging effect compensation, all the spectra were referenced by setting the hydrocarbon C1s peak to 284.80 eV.

*2.2.7 Zeta Potential*

Zeta potential measurements were performed by the streaming potential technique using an electrokinetic analyzer (SurPASS, Anton Paar) equipped with an adjustable gap cell. Two bulk samples for each glass composition (SCNB, B0, B50 and B50Sr10) were immobilized inside the measuring cell on the sample's holders, facing each other in order to create a gap (at about 100 µm) in which the electrolyte can flow during measurement [23]. 0.001M KCl was used as electrolyte for titration measurements. Its pH (initially equal to 5.6) was varied through the acid or basic range by the addition of 0.05M HCl or 0.05M NaOH respectively, by the instrument automatic titration unit. Two different sets of samples were used for acid/basic titrations to avoid artifacts due to glass reactions during the tests. In order to perform measurement at constant physiological pH (7.4) SBF, prepared according to [20], was dropwise added to ultrapure water up to pH≅7.4 and conductivity k≅18 $mS \cdot m^{-1}$ and used as electrolyte for the measurement.

*2.2.8 Contact Angle*

Surface wettability was measured by the static contact angle measurement. A drop (5 µl) of ultrapure water was deposited on the surface of the samples by means of a micropipette. The drop image was acquired through a heating microscope (Misura, Expert System Solutions) at room temperature and the contact angle measured by Image J software. At least 3 measurements per glass type were performed.

*2.2.9 Antioxidant Activity*

The scavenging potential of each glass was assessed by EPR/spin trapping by using the 5,5-dimethyl-1-pyrrolineN-oxide (DMPO) as the spin trapping agent. The decrease of the [DMPO-OH] • signal intensity was employed as an index of the scavenging activity of the bioactive glasses. The evaluation was carried out following the procedure reported in [18]. Glass powder (15 mg) was suspended in a phosphate buffered solution (pH = 7.4) containing 200 µL of DMPO 0.17 M. The suspension was irradiated with a 500 W mercury/ xenon lamp UV lamp (Oriel Instruments) equipped with an IR water-filter to avoid the over-heating of the suspension. A filter with a cut-off at 315 nm was applied to assure the energy condition necessary to induce $H_2O_2$ photolysis and prevent at the same time the photo-degradation of the DMPO

molecule. After 10 and 30 minutes of irradiation, the suspension was filtered (pore diameter 0.2 μm) and analyzed by EPR spectroscopy. The spectrum was recorded with a X-band EPR spectrometer (Miniscope 100, Magnetech, Germany). A $H_2O_2$ solution without glass powder was used as reference sample for photolysis and two high-surface amorphous silica powders (Aerosil 50 and Aerosil 150, Evonik; surface area = 50 $m^2/g$ and 150 $m^2/g$, respectively) were used to investigate the possibility that the antioxidant activity depends on a radical annealing at particle surface. Each experiment was performed in triplicate. The amount of radical generated was obtained by double-integration of the EPR signal and data were statistically analyzed with OriginPro 2018 software (OriginLab, MA, USA) by using the one-way ANOVA test and the Tukey's post-hoc analysis. Results were considered as significant for $p < 0.05$

*2.2.10 Biological evaluation*

Specimens cytocompatibility was tested towards the human osteoblasts' progenitor cells hFOB 1.19 (ATCC CRL-11372, from LGC Standards) intended as *in vitro* model of cells deputed for the scaffolds' repopulation in the self-healing process. Cells were cultivated in a HAM's F12-DMEM mix (50:50, from Sigma) supplemented with 10% fetal bovine serum (FBS, from Sigma), 1% antibiotics (penicillin/streptomycin) and 0.3 mg/ml neomycin (G418 salt from Sigma) at 34°C, 5% $CO_2$. Cells were cultivated until 80-90% confluence, detached by trypsin-EDTA and used for experiments.

- *In vitro Cytocompatibility evaluation*

Cells were dropwise seeded directly onto specimens' surface at a defined density ($2x10^4$ cells/specimen) and allowed to adhere and spread for 2 hours at 34°C, 5% $CO_2$; then, specimens were submerged with fresh medium (1 ml/specimen) and cultivated for 48 and 72 hours. At each time-point the viability of surface-seeded cells was evaluated by the metabolic colorimetric assay alamar blue (alamarBlue, ready-to-use

solution from ThermoScientific) following Manufacturer's instructions: briefly, supernatants were removed and replaced with 1 ml of the alamar solution that was incubated for 4 hours in the dark (34°C). Afterwards, 100 µl were removed, spotted into a new black 96-well plate and fluorescence signals were evaluated with a spectrophotometer (Spark, Tecan Trading AG) using a fluorescence excitation wavelength 570 nm and a fluorescence emission reading 590 nm. Moreover, the adhesion, spread and morphology of cells cultivated onto specimen surface was visually checked by digital light microscopy (Invitrogen EVOS Floid, from ThermoScientific) after 72 hours cultivation. Results were compared to polystyrene that was considered as gold standard and 100% viability; results are presented as relative fluorescent units (RFU).

- *Scavenger activity evaluation*

To test the bioactive glasses potential antioxidant scavenger activity, the level of oxygen and nitrogen active species was evaluated in the supernatant by means of a colorimetric assay (In Vitro ROS/RNS Kit Assay from Cell Biolabs) which is based on the free radical capacity of oxidize the non-fluorescent molecule dichlorodihydrofluorescine (DCFH) by converting it into the dichloroflorescine (DCF) fluorescence molecule. The values were collected in physiological bulk conditions after 3 days immersion in fresh medium and after inducing oxidative stress by adding 500 mM hydrogen peroxide 3 hours/day [19]. Briefly, 50 µm of supernatant were transferred to a 96-well plate with black walls and mixed with 50 µm of catalysis (1: 250 in PBS) for 5 minutes at room temperature; after 5 minutes, 100 µm of DCFH solution were added to each well, and after 40 minutes fluorescence was analyzed using a spectrophotometer (Spark, Tecan Trading AG) with a wavelength of 530 nm. To test the scavenger protective effect of the glasses, cells were cultivated onto specimens' surface as previously described in the cytocompatibility assay and their viability has been evaluated by the alamar blue assay in physiological and oxidative stress conditions after 3 days. Polystyrene was considered as control in both experimental conditions.

- Statistical analysis of data

Experiments were performed using three replicates. Normal distribution and homoscedasticity were tested with Wilk-Shapiro's and Levene's test, respectively. Samples were statistically compared by the SPSS software (v25, IBM, New York, NY, USA) using the one-way ANOVA test and the Tukey's post-hoc analysis. Results were considered as significant for $p < 0.05$

## 3 Results and Discussion

### *3.1. Density Test and Molar Volume*

The density and the molar volume, reported in Table 3, were calculated by using the formulas reported in section 2.2.1, after weighting 2 samples for each glass composition in air ($w_{air}$) and ethanol ($W_{eth}$). The results of standard deviations calculation were ±0.02.

**Table 3**: density and molar volume of the glass samples

| | **ρ [g/cm³]** | **$V_m$ [cm³/mol]** |
|---|---|---|
| **SCNB** | 2.66 | 22.50 |
| **B0** | 2.65 | 23.05 |
| **B50** | 2.61 | 24.39 |
| **B50Sr10** | 2.77 | 24.45 |

Density and molar volume give information about the influence of different cations on the silicate structure. Atomic weight and radius of the substituted cations affect molar volume and density, and can lead to an expansion or a contraction of the silicate network. It has been demonstrated that density plays an important role in properties such as solubility and bioactivity [18, 24-27]. The density and the molar volume variations in the bioactive glass samples, reported in table 4, show that density does not change by adding $P_2O_5$ in substitution to silica oxide, while the molar volume increases, suggesting an expansion of the glass network. The substitution of boron oxide, in place of silicon dioxide, leads to an increase of the molar volume, and to a simultaneous decrease in density. Boron has a lower atomic weight than the average mass of the glass constituent, and this results in a decrease in density. Furthermore, boron ions are likely to form B-O-Si diborate and non-bridging oxygen (NBOs) in the glass structure, resulting in an increase of the free volume within the glass. The increase in the molar volume might be correlated with the preferential formation of a borate phase, immiscible with the silicate phase, leading to the expansion of the overall glass network [28,29]. Replacing SrO/MgO for CaO causes an appreciable increase in density, due to the

higher Sr atomic weight when compared to Ca, compensated by the larger size of the $Sr^{2+}$ cation compared to $Ca^{2+}$, that tends to expand the glass network.

*3.2 Raman Spectroscopy*

Raman spectroscopy was carried out on bulk samples not soaked in any buffered solution. The spectra for each glass composition are shown in Figure 1. The observations presented below were obtained on the basis of literature articles [30, 31]. From SCNB and B0 spectra it is possible to see clearly the typical vibration peaks and bands of the bioactive glasses: peak at ~ 613 $cm^{-1}$ can be related to the Si-O-Si bond rocking vibrations, where the oxygen atoms move perpendicularly to the Si-O-Si plane; the small band between 750-800 $cm^{-1}$ is associated to the Si-O-Si bending vibrations, where oxygen atoms move to and from the two adjacent Si atoms in the Si-O-Si plane; the band between 900-980 $cm^{-1}$ is related to the modes of non-bridging oxygen (NBO) atoms; band at 1000-1200 $cm^{-1}$ is attributed to the vibrations of bridging oxygen atoms (bond stretching vibrations), where the BO's move parallel to the Si-Si lines in the opposite direction to their Si neighbors. Peak at ~ 613 $cm^{-1}$ is more intense in SCNB compared to the B0 one, as well as the band between 1000-1200 $cm^{-1}$, since SCNB has more Si in its network. The asymmetry in the shape of the B0 band at ~ 1080 $cm^{-1}$ is a vibrational indicator of the network disruption. Lastly, the frequency shifts of both B0 non-bridging and bridging oxygen bands is ascribable to the change of the $SiO_2$. With respect to the B50 and B50Sr10 spectra, we can make the following considerations: wavenumbers in the 550-850 $cm^{-1}$ region are characteristic of ring breathing modes, in particular band at ~ 670 $cm^{-1}$ can be associated to tetraborate groups, whereas bands at 770 $cm^{-1}$ and 808 $cm^{-1}$ correspond to the four- and three-coordinated boron in diborate and boroxol rings, respectively. Peak at ~ 580 $cm^{-1}$ may be associated to the borosilicate rings. The band between 950-980 $cm^{-1}$ is assigned to the NBO, consisting of Si-O- stretching in structural units with one or two non-bridging oxygens per silicon (Q3 , Q2); wavelengths from ~ 1000 $cm^{-1}$ to ~ 1050 $cm^{-1}$ are attributed to the Si-O- bridging oxygen stretching modes; broad band between 1250 and 1500 $cm^{-1}$ has been assigned to B-O- stretching in chain-type metaborate groups; particularly, the component centered at ~ 1480 $cm^{-1}$ is related to $BO_3$ units bonding $BO_3$ units. Bands

concerning NBO and BO vibrational modes are less intense in borosilicate glasses compared to SCNB and B0, because of the presence of boron in the structural network.

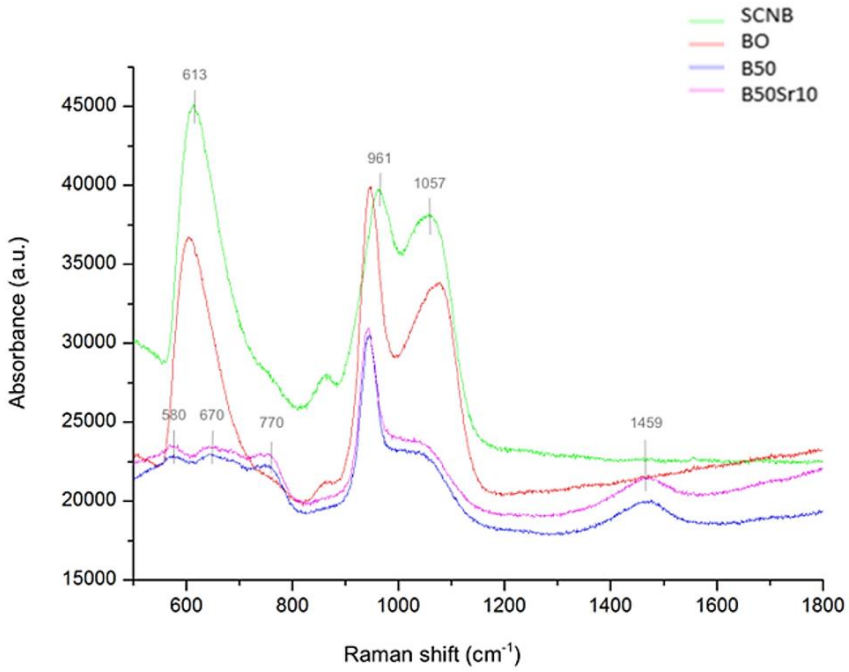


***Figure 1:*** *Raman spectra of bulk samples not soaked in any buffered solution.*

*3.3 Mass Loss*

The change of weight is a sum of the glass dissolution (weight loss) and reactive layer precipitation (weight gain). All the compositions show a mass change in both the solutions. In Figures 1.a and 1.b it is possible to observe that in Tris, as well as in SBF, B50Sr10 and B50 follow the same trend and the most appreciable mass loss, significantly differing from the other two glasses; this marked dissimilarity can be explained by the faster dissolution rate of the Borate phase, in borosilicate bioactive glasses, and the expanded network of the borate glasses. Moreover, the slight increase in network expansion (due to P presence) of the B0, compared with the SCNB, results in a slight increment of the mass loss. It is interesting to point out, that, overall, the mass loss is greater in TRIS than in SBF. This can be correlated with the higher probability of

inducing a reactive layer precipitation in SBF than in TRIS buffer solution, due to the tendency of SBF to be supersaturated toward the precipitation of an apatite layer [32].

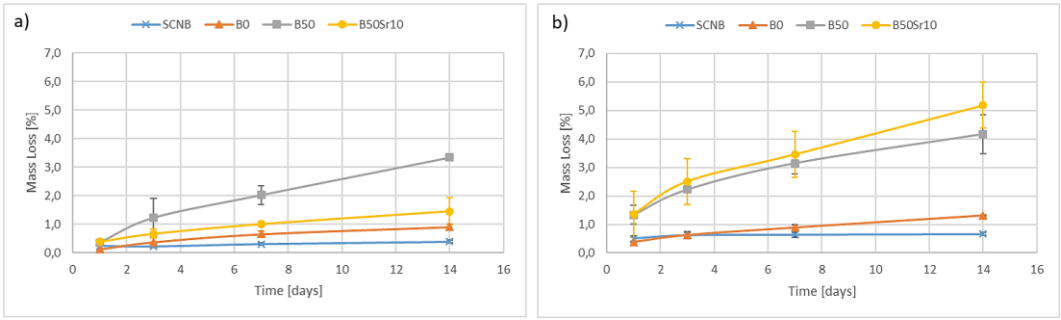


***Figure 2****: mass loss percentage of the bulk samples soaked for increasing time in SBF (a) and in TRIS (b).*

*3.4 pH Measurement*

Figure 3.a and 3.b describe the pH values measured for the bulk samples. As expected from silicate and borosilicate bioactive glasses, with an increase in immersion time the pH increased. This is associated with ions leaching from the glass to the solution and the exchange of $Na^+$ with $H^+$, as reported by L.L. Hench [3]. In agreement with the mass loss results, it is apparent that, regardless of the glass composition, the pH rise is higher in Tris than in SBF. Also, at long immersion time the pH is higher when P is added to the glass (SCNB vs. B0) or when $SiO_2$ is partially replaced by $B_2O_3$ (B0 vs. B50). This indicates that not only the lower hydrolytic resistance of the borate phase induced an increase in the dissolution rate, but also the increase in the network molar volume.

While in Tris the substitution of Sr and Mg for Ca, in the glass composition (B50 vs B50Sr10) seems not to cause significant changes in the pH (according to the Anova test), in SBF the B50Sr10 reveal to have lower pH than B0 and B50. It is noteworthy that the solution used for the in-vitro dissolution has an impact on the dissolution mechanism. Indeed, as shown in [33] immersion in SBF, generally leads to a lower increase in pH than when immersed in TRIS buffer solution. From figure 3b one can assume that the substitution of Sr and Mg for Ca stabilizes the glass network and therefore increase the hydrolytic resistance, as previously shown [33, 34].

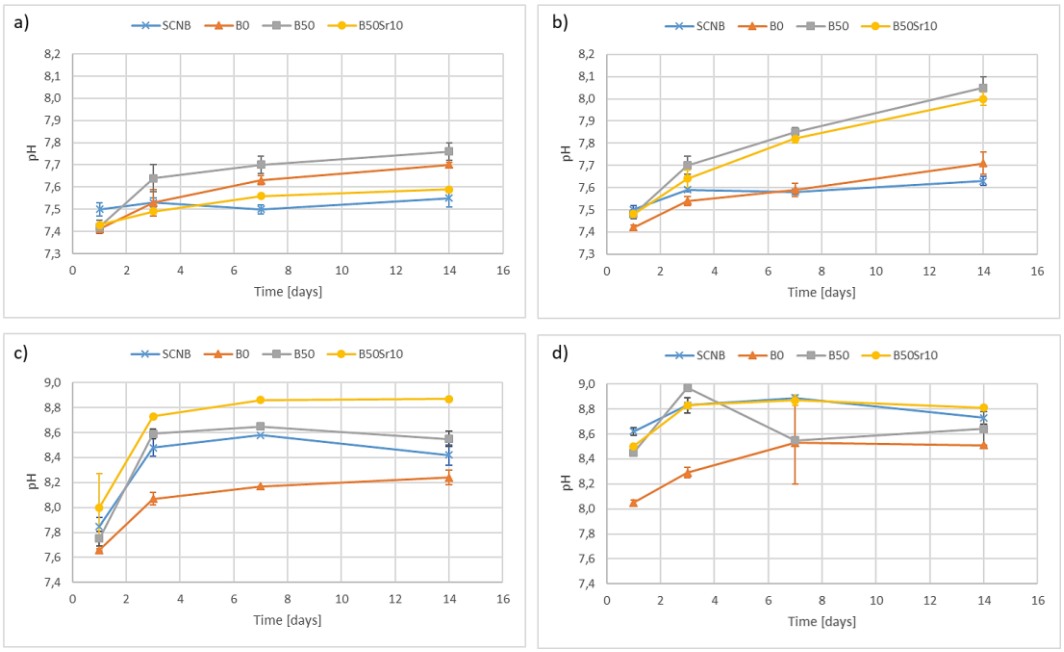


***Figure 3**: pH variations of the bulk samples soaked for increasing times in SBF (a) and in Tris (b) and of powder samples soaked for increasing times in SBF (c) and in Tris (d).*

Figures 3c and 3d describe the pH values measured for the powder samples. The pH trends of the glass powders reveal significant differences from those seen for the bulks. As a matter of fact, the resulting pH depends on the particle size and on the concentration of the glass in solution, as well as on the buffering capacity of the surrounding liquid. The pH reached, in both SBF and Tris, is considerably higher than the one seen in the bulk samples: this marked increment can be explained with the small particle size of the powders (<38 µm), exposing a large surface area available to the buffered solutions, and therefore increasing the dissolution rate, as reported in previous studies [18]. All the compositions clearly show pH rise within the first 24h of immersion in both SBF and Tris buffer; moreover, there is a further increase in pH between 24h and 3 days followed by a stabilization, suggesting that the precipitation of HCA on the surface occurs within the first 3 days. Two exceptions have been observed in the behavior described in the previous point: B0 shows an important increment of the pH until 7 days, while B50 undergoes to a decrease of the pH at 7 days; the pH differences between the four compositions are less evident in powder samples

in comparison with bulks, since the pH changes in a smaller range of values; B0, B50 and B50Sr10 trends are consistent with what has been said about the network expansion in bulk samples: borate glasses show a higher dissolution rate, due to the boron presence.

*3.5 Ion Release in SBF and Tris: ICP-OES*

Since pH and mass loss result from the competition between dissolution and precipitation, they cannot completely describe the dissolution rate. At this purpose ion release can better evidence the dissolution of the glass backbone.

ICP-OES analysis were done on SBF and Tris solution, post-immersion. The element concentrations, as a function of time, are shown in Figures 4 and 5 for bulk and powders samples respectively. It is important to remind that the release of ions in SBF is complicated by those already present in the solution, but also by the apatite formation which consumes ions such as $Ca^{2+}$, $Sr^{2+}$ and $PO_4^{3-}$. This accounts for the differences between results obtained for Tris and SBF.

*3.5.1 Bulk Samples*

From the analysis of the release curves in SBF, reported in Figure 4.a, 4.c, 4.e, 4.g, we can observe that B50 releases more boron ions if compared with the B50Sr10, by confirming the role of Sr and Mg in reducing the glass dissolution. All the compositions exhibit a decrease in phosphorous ions, correlated with the precipitation of hydroxyapatite on the glass surface. After 14 days, phosphorous, dissolved from the glass and contained in the solution, is completely consumed in SCNB, B0 and B50, while B50Sr10 shows a small decrement of the P ions; this behavior can be imputable to the lower Ca content in B50Sr10, corresponding to an increase in the network connectivity, and therefore to a significant reduction of the glass dissolution, ion release and apatite formation [24]. The lower level of phosphorous have been detected for the SCNB glass immersed in SBF, since the only P ions participating to the HCA formation are those contained in the solution. B0 and B50 are composed by the same amount of P, but the higher solubility of boron causes a greater initial ion release, leading to an increase of the P concentration and a delay in the phosphorus precipitating into an HCA layer. Ca release is nearly constant with time in B0 and B50Sr10, while decreases

in SCNB, since the formation of the HCA layer consumes Ca ions taken from the SBF solution. An increment of Ca levels has been measured also in B0, due to the faster dissolution rate of boron; and the predominant affinity of Ca with the borate phase [29]. From Si variation it is clear that the Sr substitution induces a lower dissolution rate of borate glasses. Despite the more open network of B50 and its greater solubility, it contains less Si in its network resulting in a lower Si release in comparison with B0.

By observing the release curves in Tris, reported in Figure 4.b, 4.d, 4.f, 4.h, it is possible to say that the concentration of boron released is equal for B50 and B50Sr10, in contrast with the trends shown in SBF, indicating once again how in Tris the main appreciable effect is the different expansion of the network. For all the compositions, Ca and P initial values, and consequently the final ones, are substantially lower compared to those measured in SBF, since no Ca and P ions are contained in Tris solution. For the same reason (absence of ions in Tris), Ca concentration increases with time in all our glasses. In B50Sr10, phosphorous and calcium are subjected to the same changes seen in SBF solution (lower decrease in P and lower increase in Ca), because of the lower Ca content in the glass.

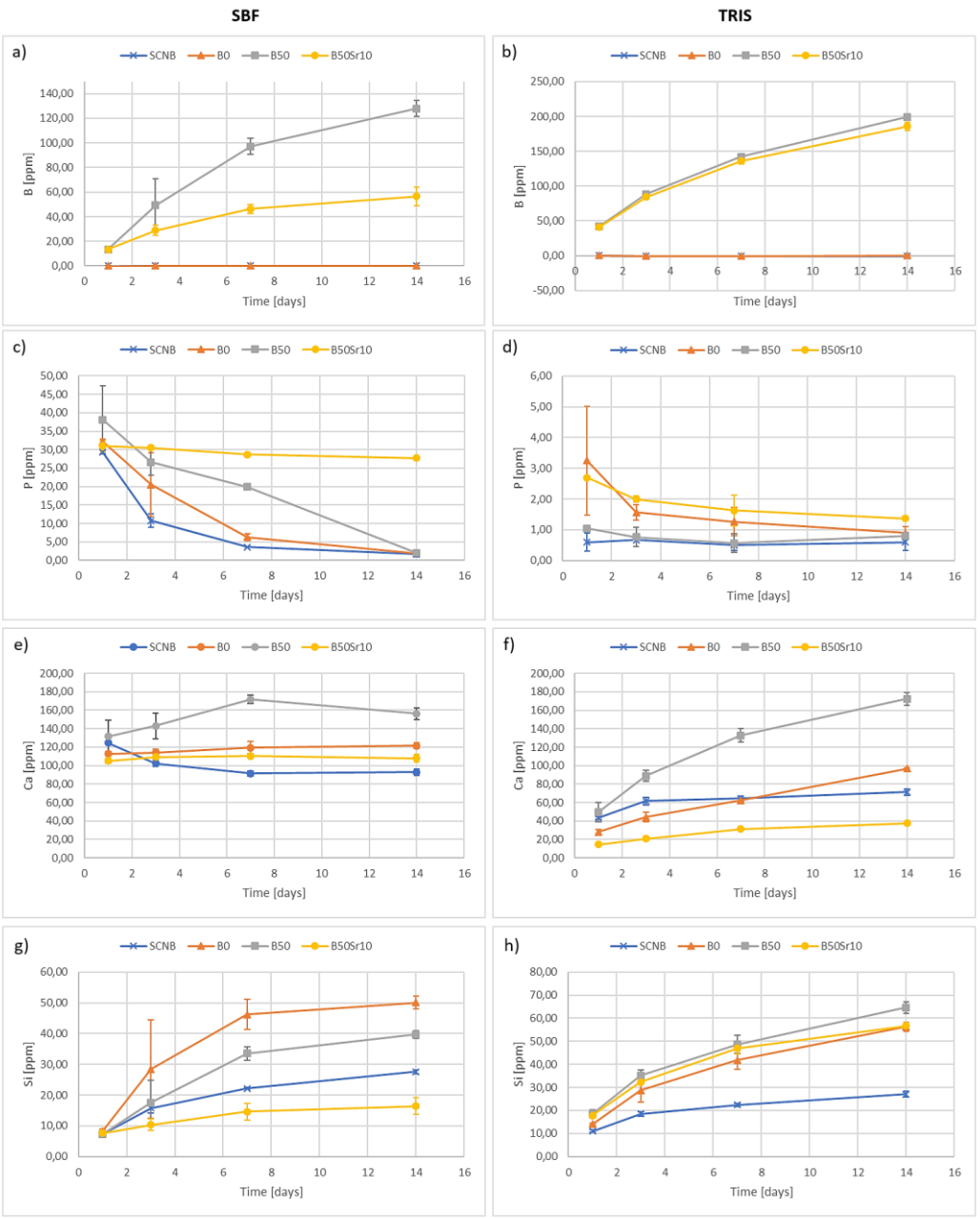


***Figure 4****: B, P, Ca and Si release from bulk samples soaked for increasing times in SBF and in Tris.*

*3.5.2 Powder Samples*

As reported for the pH, the dissolution behavior and therefore ions release in solution appears significantly different with respect to the bulk samples.

In the release profiles in SBF (Figures 5.a, 5.c, 5.e, 5.g), considering the P and Ca concentrations, it is clear that the precipitation of hydroxyapatite on the glass surface happens in the first three days of immersion: P decreases drastically by reaching values around zero after three days, while Ca remains constant (B0 and B50Sr10) or even decreases (SCNB and B50). This suggests that powders induce a faster precipitation of HCA on the particle surfaces by consuming P and Ca ions both presented in the solution and release consequently the degradation of the glass surface. The initial increase of Ca levels in B50 is caused by the faster solubility of B. The B0, B50 and B50Sr10 trends confirm the considerations done for the bulk samples on the network expansion and the role of Sr and Mg, even if Sr and Mg seem to not affect boron and silicon release. Lastly, it was also measured a decrease in Mg levels (data not shown), not only in the composition containing Mg (B50Sr10) but also in those glasses lacking in it, that has been correlated to the fact that the HCA precipitation assimilates also a small but significant percentage of magnesium besides P and Ca.

In Tris solution (Figures 5.b, 5.d, 5.f, 5.h), the behavior of the powder glasses reflected what has been said previously about powder samples in SBF. The precipitation of HCA occurs in the first three days, even if it does not happen suddenly as in SBF, and the initial concentration are lower – there are no interaction with solution ions. Silicon release does not change significantly from one glass to another, and remains nearly constant. Ca and P release show once again the influence of Sr and Mg on B50Sr10 with respect to the B50.

The fast reactivity of powders in respect to bulk samples could be ascribed to the higher surface area to volume ratio, that is likely to increase the speed of ion release [35-37].

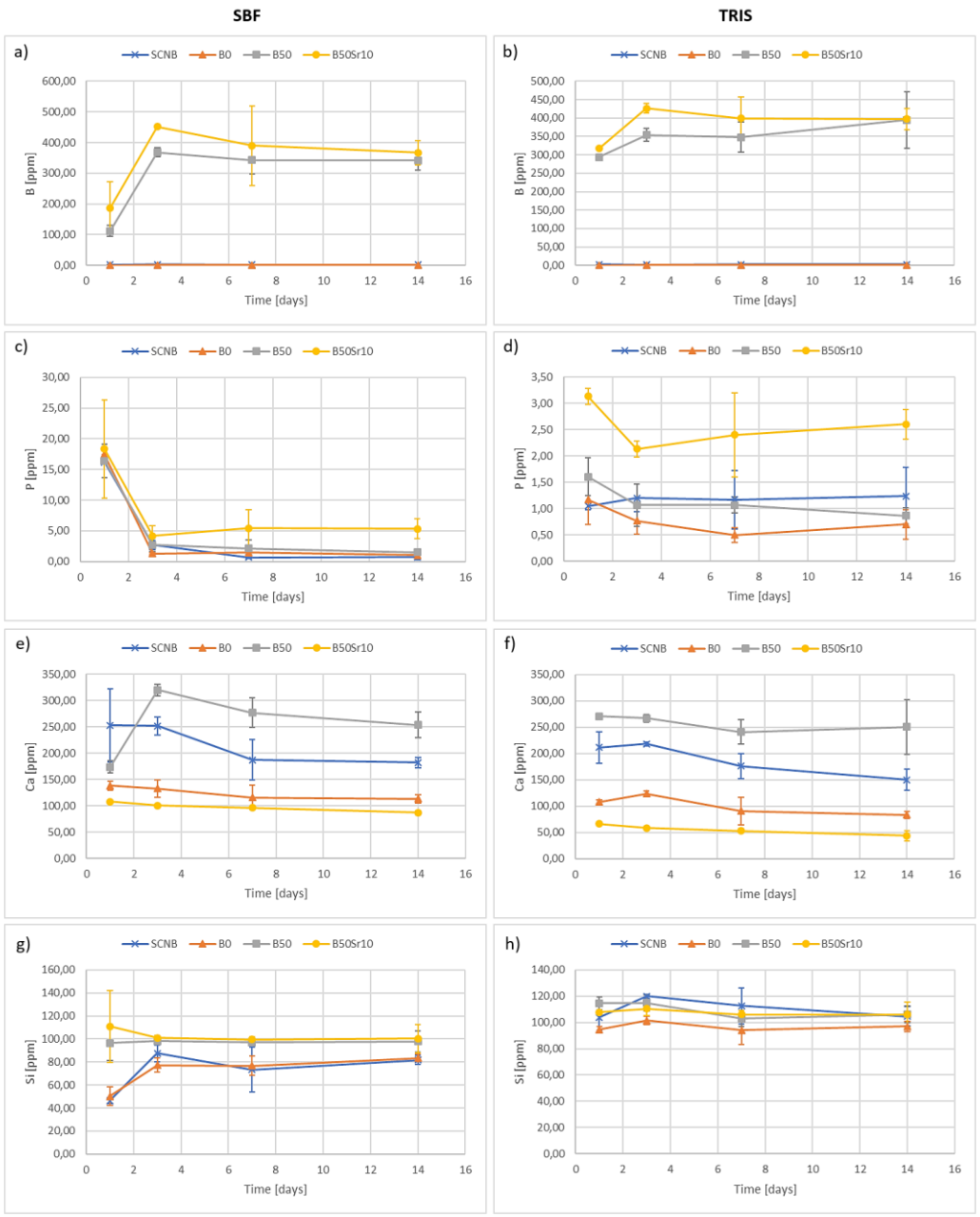


***Figure 5****: B, P, Ca and Si release from powder samples soaked for increasing times in SBF and in Tris.*

*3.6 Fourier Transform Infrared Spectroscopy (FTIR)*

FTIR was performed on bulk samples before and after immersion in both SBF and Tris buffered solutions. Figures 6 and 7 show the obtained results. The analysis on not soaked samples (Figure 6) shows the spectra of the boron free compositions and spectra of the borosilicate B50 and B50Sr10 glasses.

Peaks in SCNB and B0 spectra have been identified as following: band at ~ 740 $cm^{-1}$ is attributed to the bending mode of Si-O-Si bonds [38]; band at ~ 910 $cm^{-1}$ is associated to the stretching mode of Si-O groups

with one no bridging oxygen (Si-O-NBO) and to the silanol groups Si-OH [39-41]. The band at ~ 1020 $cm^{-1}$ represents the asymmetrical stretching (stretching mode) of both Si-O-Si in [$SiO_4$] units [39-41]. Finally, a broad band in the 1400 – 1515 $cm^{-1}$ region is also seen and corresponds to carbonate in the glass structure [42]. As opposed to the pure silicate, the borosilicate glasses exhibit a shift of the band at ~740 $cm^{-1}$ to 711 $cm^{-1}$. A broadening of the band at 910 $cm^{-1}$ with the likely appearance of a shoulder at 838 $cm^{-1}$. Finally, new bands at 1204 and 1387 $cm^{-1}$ are also visible in the borosilicate glasses. Borate glasses are mainly composed of $BO_3$ triangle and $BO_4$ pyramidal groups, therefore, spectra peaks are assigned to B-O bonds of the both groups, and they can be identified as: band at ~ 715 $cm^{-1}$ is associated to the B-O-B bending linkage [43-45].The [$BO_4$] units, and the broadening of the main band can be attributed to the combination of [$BO_4$] at 875 $cm^{-1}$, B-O-M (where M is a cation) at 992 $cm^{-1}$, as well as B-O-B and B-O-Si linkages [43-45]. The region between 1200 and 1400 $cm^{-1}$ is characteristic of the B-O stretching vibrations of [$BO_3$] units in pentaborate, pyroborate and orthoborate groups. In particular, band at ~1227 $cm^{-1}$ and shoulder at ~1337 $cm^{-1}$ are correlated to the [$BO_3$] triangles and the [$BO_2O^-$] groups, while the peak at ~1380 $cm^{-1}$ is typical of the [$BO_3$] triangles [43, 44]. As expected, the substitution of CaO for SrO in the borosilicate glass does not induce significant structural changes [46]

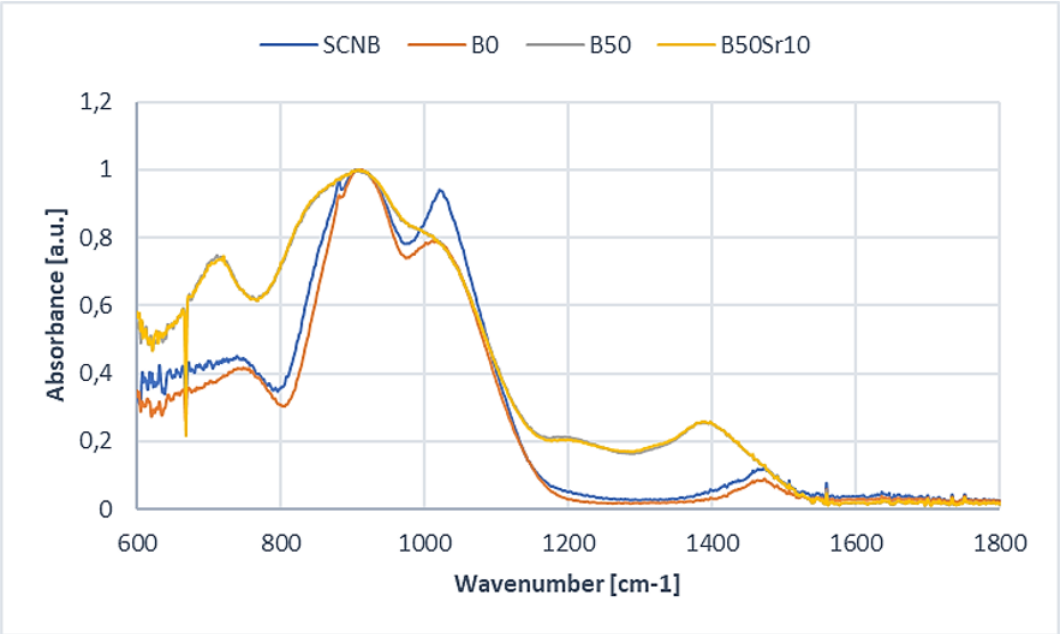


***Figure 6****. FTIR analysis of the bulk samples not soaked in buffered solution.*

The spectra variations after the sample immersion are similar in SBF and Tris, and by observing Figure 7 two differences between the samples soaked in SBF and Tris are noticeable: the peak associated to the [$PO_4^-$] groups, and therefore to the hydroxyapatite precipitation (~1035 $cm^{-1}$) is less pronounced in Tris in comparison with SBF, confirming the pH and ICP-OES results; furthermore, in Tris the peak related to the formation of a 3D silica-like structure is more pronounced for the SCNB composition.

Concerning samples immersed in SBF solution, the changes in the glass surface composition can be described as follow. All glasses show a decrease of the signal at ~ 930 $cm^{-1}$ with the increase of the immersion time, revealing a decrement of [$SiO^-$] and [$SiO_4$] units. Appearance of the shoulder at ~870 $cm^{-1}$ confirm the presence of phosphate vibrations, since it can be attributed to the P-O vibration modes. The presence of the shoulder at ~ 960 $cm^{-1}$ may be attributed to C-O vibration modes in [$CO_3^{2-}$] groups and to P-O-P bonding. Bands at 715 and 780 $cm^{-1}$ disappear, while a new peak at ~ 790 $cm^{-1}$ clearly shows up, assignable to the vibrational mode of Si-O-Si between two adjacent silica tetrahedrons, resulting from the condensation reaction. After 24h, the band between 930 and 1020 $cm^{-1}$ increase, sharpen, and shift to a higher wavenumber; the peak, associated with the P-O stretching modes of [$PO_4^-$] groups, appears at ~1035 $cm^{-1}$. The presence of carbonate groups is further confirmed by the intensity increase of the band at 1350-1550 $cm^{-1}$, becoming even more intense with time. Peak at ~ 870 $cm^{-1}$ change gradually in a more pronounced shape with time. Band at ~1200 $cm^{-1}$ is caused by to the vibrational modes of Si-O-Si in the silica gel at the interface between the glass and the precipitated layer. The peak at ~ 1035 $cm^{-1}$ becomes more intense and pronounced with the increasing of the time immersion as well as the typical peak associated to [$CO_3^{2-}$] groups. In borate glasses (B50 and B50Sr10), bands in the 1200-1600 $cm^{-1}$ region, typical of the borate network, are substituted with the carbonate group doublets at 1350-1550 $cm^{-1}$. After the initial immersion, borate glasses show a split of the broad band between 800 and 1150 $cm^{-1}$ into three well defined bands centered at ~ 1009, 950 and 870 $cm^{-1}$. The higher intensity of the [$CO_3^{2-}$] region at 1350-1550 $cm^{-1}$ and the lower intensity of the shoulder at 1220 $cm^{-1}$ indicate a thicker and more crystallized HCA layer at the glass surface; therefore, FTIR confirm the pH and ICP-OES data, since in B50Sr10 is the less

reactive glass (surface structural modification occurs less rapidly and the HCA layer is thinner and less crystallized), followed by the SCNB, whereas the reactivity increase in B0 and B50.

Further considerations can be done by comparing the FTIR spectra of samples immersed in SBF with those obtained for samples soaked in Tris. The main difference is that phosphate and carbonate vibration modes are considerably less pronounced in Tris than in SBF, because of the different composition of the solutions: SBF contains a significant amount of Ca and P, and thus, it tends to saturate faster and forms a thicker HCA layer, while the lack of ions in Tris leads to a more sustain glass dissolution and to a delayed layer formation. FTIR results mainly evidence the precipitation of a Ca/P layer, which can be associated to hydroxyapatite precipitation also looking at previous data published by the authors on glasses with analogous compositions [47, 48].

All these observations are supported and confirmed by the ICP-OES and pH measurement results.

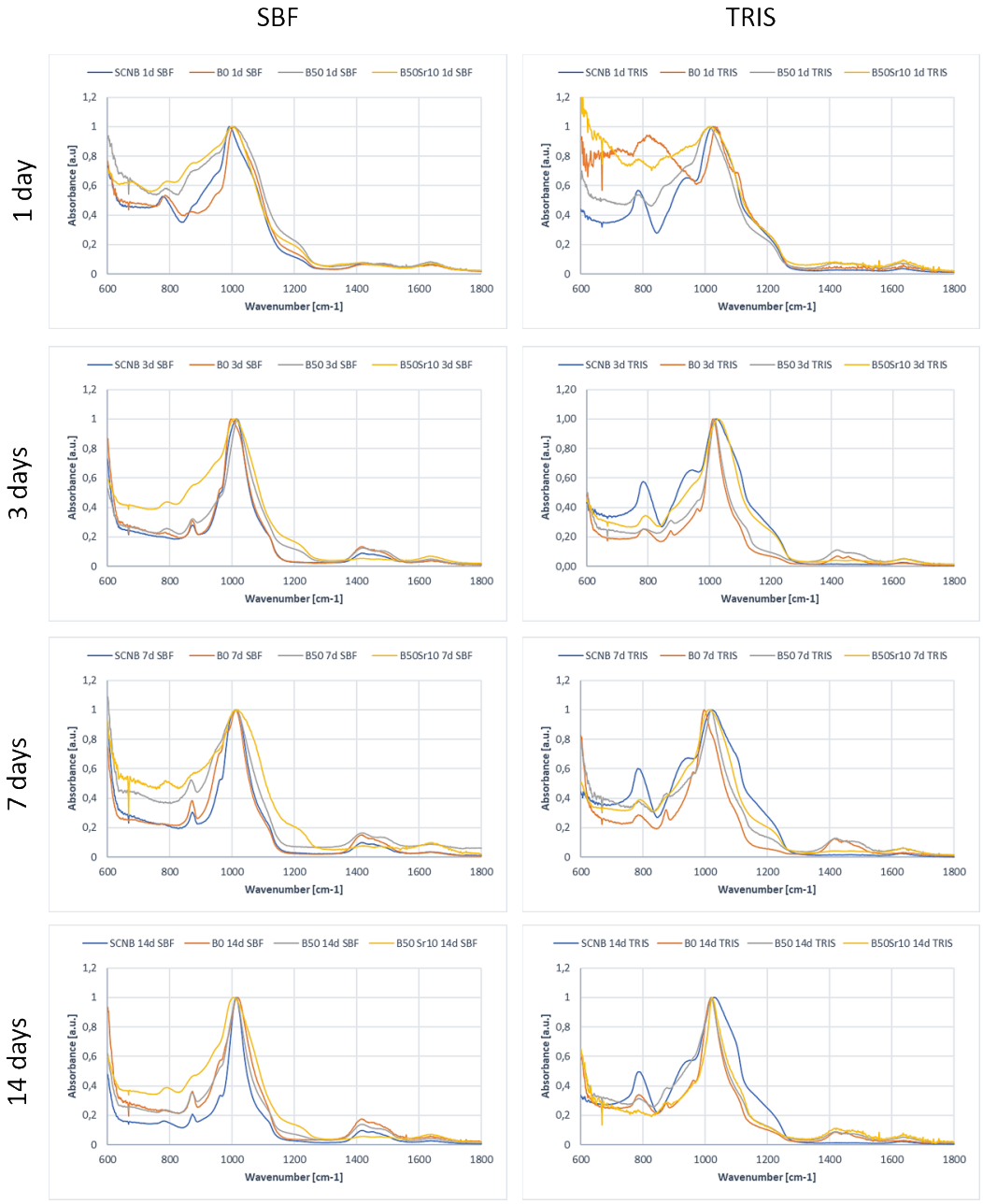


***Figure 7**: FTIR analysis of the bulk samples after increasing times of soaking in SBF and in TRIS.*

*3.7 X-ray Photoelectron Spectroscopy (XPS)*

The XPS analysis was implemented to characterize the chemical composition and the fundamental bonds on the glass surfaces [49,50]. The full spectrum analysis performed to identify the atomic percentages of the single glass constituents, through the XPS Survey analyses in the range 0-1200 eV (data not shown), revealed a good correspondence to the compositions reported in table 1.

A more accurate analysis (high resolution spectra) was implemented in order to investigate the oxidation state and the chemical neighborhood of the elements found with the Survey spectra and study the type of the chemical functional groups/bonds composing the first layers of the material (4-5 nm). Three regions were investigated: carbon, oxygen and silicon regions (Figures 8.a-h).

As explained in the materials and methods section, polished and washed surfaces were considered for the XPS analyses since they are the ones considered for the other characterization and can help understanding the role of surface functional groups on glass behavior (mainly antioxidant ability). In these conditions a certain amount of carbon contaminants can be detected on the surface due to material reactivity. As a confirmation, in the carbon region (Figure 8.a-d) the main signal is at 284.5 eV and can be associated with C-C and C-H bonds of hydrocarbon contaminants, always present on reactive surface [51, 18, 19]. A signal with moderate intensity, appears at 286 eV, it is ascribable to C-O bonds [18] and can be associated to carbon contaminations. The peak at 289 eV can be attributed to carbonates [18, 52] and is related to surface carbonation of bioactive glasses, frequently observed [18, 52], and the C-O and carbonate peaks increase in borate glasses. This increment is easily explainable considering that any surface exposed to environmental air is affected by adventitious carbon from the environment and its amount is directly related to the reactivity of the material with ambient air. Bioactive borosilicate glasses are more reactive than their silicate counterpart and therefore it is not unreasonable to find an increase in the C-O contamination when replacing part of the $SiO_2$ with $B_2O_3$.

The Si region (spectra not reported) presents a single contribution for all the tested glasses. It is centered at about 102.9 eV for SCNB and B0 and at about 102.5 eV for B50 and B50Sr10. The signal can be attributed to Si-O bonds in $SiO_2$. These results can be explained considering that in pure silica the Si-O binding energy is around 103.2 and when increasing the content of alkaline and alkaline earth (at the expense of the $SiO_2$) the binding energy shift to 102.9, for typical silicate bioactive glass [53]. For this reason, a shift toward lower binding energy for the borosilicate glass is expected, since the content in alkaline and alkaline earth remain the same but the silica content decrease.

In the oxygen region (Figure 8. e-h) two main contributions at about 530 eV and 532 eV can be observed for all the tested glasses. The first signal can be attributed to silica and metallic oxides, while the second one to OH groups [54] The ratio between the intensity of the OH signal and the oxides one has been calculated and inserted in Figure 8. It can be noted that SCNB present the highest hydroxylation degree among the tested glasses.

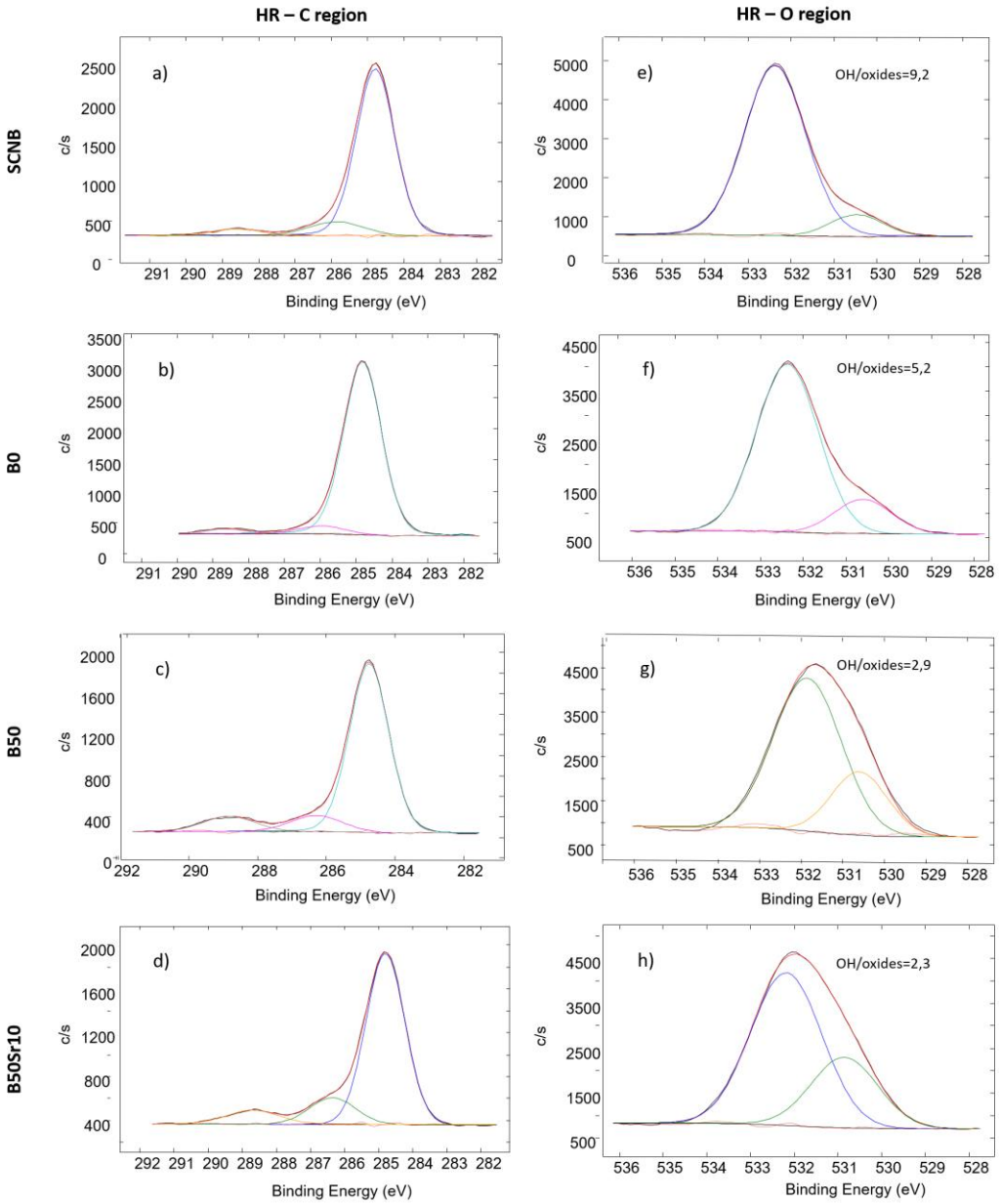


***Figure 8**: XPS high resolution spectra of the investigated glasses. a-d carbon region, e-h oxygen region*

*3.8 Zeta Potential*

Table 4 reports the zeta potential values measured on the samples in contact with SBF or KCl solutions at the physiological pH, together with the isoelectric point values (IEP) extrapolated from the titration curves obtained on the samples in contact with KCl.

The aims of the titration curves in KCl are to evaluate eventual difference of the surface zeta potential of the glasses as a function of pH, to measure the isoelectric point (IEP), and to compare the zeta potential of the different glasses at physiological pH. The zeta potential at physiological pH was also measured in diluted SBF in order to simulate a chemical environment much closer to the physiological one; zeta potential, in fact, can be affected by the ionic strength of the solution. The IEP was not identified during the acid titration since the glasses are characterized by high reactivity, and they reacted with the electrolyte during the analysis. Thus, the measurements registered for pH values smaller than 3.5 are not significant. However, it is possible to estimate the IEP value by extending the line obtained before the reaction between the glass and the solution (Table 4).

**Table 4**: Results from the zeta potential measurements in diluted SBF and titration curves in KCl

| | ζ@pH=7.4 (SBF) | ζ@pH=7.4 (KCl) | IEP (KCl) |
|---|---|---|---|
| SCNB | -74 | -70 | 2-2.5 |
| B0 | -50 | -60 | 2-2.5 |
| B50 | -33 | -27 | 2.5 |
| B50Sr10 | -34 | -34 | 3-3.5 |

All the glasses show an acidic isoelectric point, according to the present of acidic OH groups on their surfaces, as previously observed by the authors in similar glass compositions [18, 28]. In agreement with their acidic IEP, all the glasses are negatively charged at physiological pH, both in SBF and in KCl. No significant difference due to the ionic strength of diluted SBF was detected. Moreover, all the glasses show a plateau of the zeta potential curve in the basic region (Figure 9) which is a further index of the presence of acidic functional groups on the surface. The onset of the plateau is around pH 5-6 for all the glass

compositions, suggesting that the exposed -OH act as an acid with similar strength on all the glasses: they yield $H^+$ ions when in contact with an aqueous solution, charging themselves negatively and are completely deprotonated at any pH higher than 5-6.

The zeta potential of a surface with acidic functional groups, at pH higher than IEP, depends on the quantity (that is in this case the hydroxylation degree) and acidic strength of the functionalities. Considering that the -OH groups have almost the same acidic strength on all the glasses, the magnitude of the negative charge is expected to be related to the hydroxylation degree. The obtained zeta potential values at physiological pH are in line with the hydroxylation degree derived from the XPS analyses: higher is the hydroxylation degree (that is maximum for SCNB and minimum for B50Sr10), higher is the magnitude of the negative charge at pH=7.4.

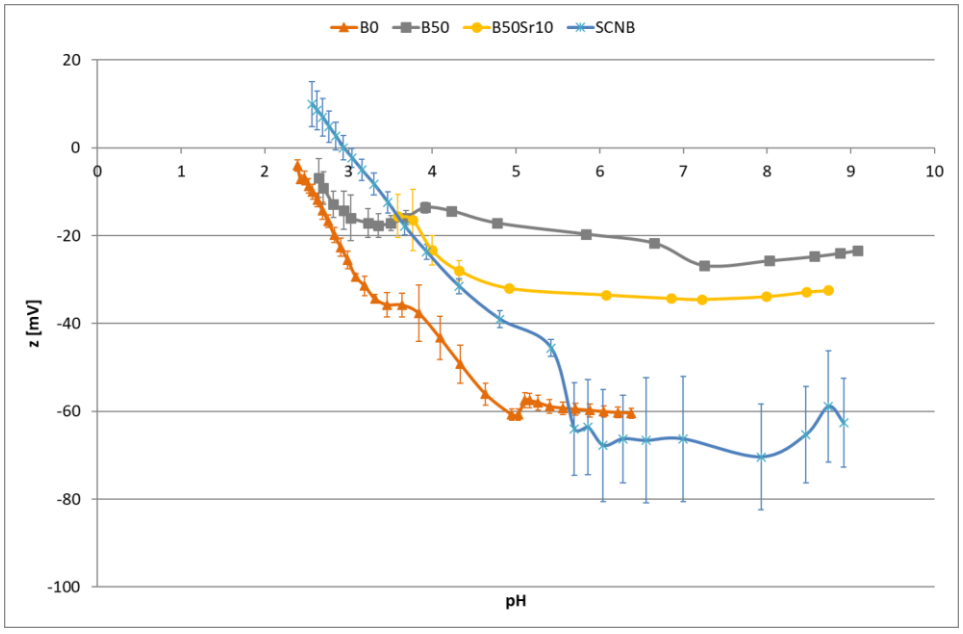


***Figure 9**: Zeta potential vs pH of the glass samples, measured with acid/basic titration.*

*3.9 Contact Angle*

The values of the contact angels measured on the tested glasses are reported in table 5. All the glasses present a hydrophilic behavior (contact angle<<90°). SCNB shows the lowest contact angle, in accordance with its higher hydroxylation degree.

**Table 5:** Contact angle measurements

| | Contact angle (mean ±standard deviation) |
|---|---|
| SCNB | 12.1 ± 0.85 |
| B0 | 43.85±1.06 |
| B50 | 44.6±1.13 |
| B50Sr10 | 46.75±3.04 |

*3.10 Antioxidant Ability: EPR Evaluation of HO• Scavenging Activity*

EPR analysis was performed on a per mass basis. Figure 10A reports the representative EPR spectra recorded after 10 and 30 minutes of irradiation of suspensions of bioactive glasses (namely SCNB, B0, B50 and B50Sr10) in comparison with a clear solution in the absence of dust employed as positive control (ctrl+) and two high surface area amorphous silica (i.e. Aerosil 50, 50 $m^2/g$ – A50, and Aerosil 150, 150 $m^2/g$ – A150) employed as models in virtue of their inertness. Figure 10B shows the mean values of the signal

intensity obtained by double integration of the EPR spectra. The columns that do not share same letters are considered statistically different (ANOVA, Tukey's test p <0.05).

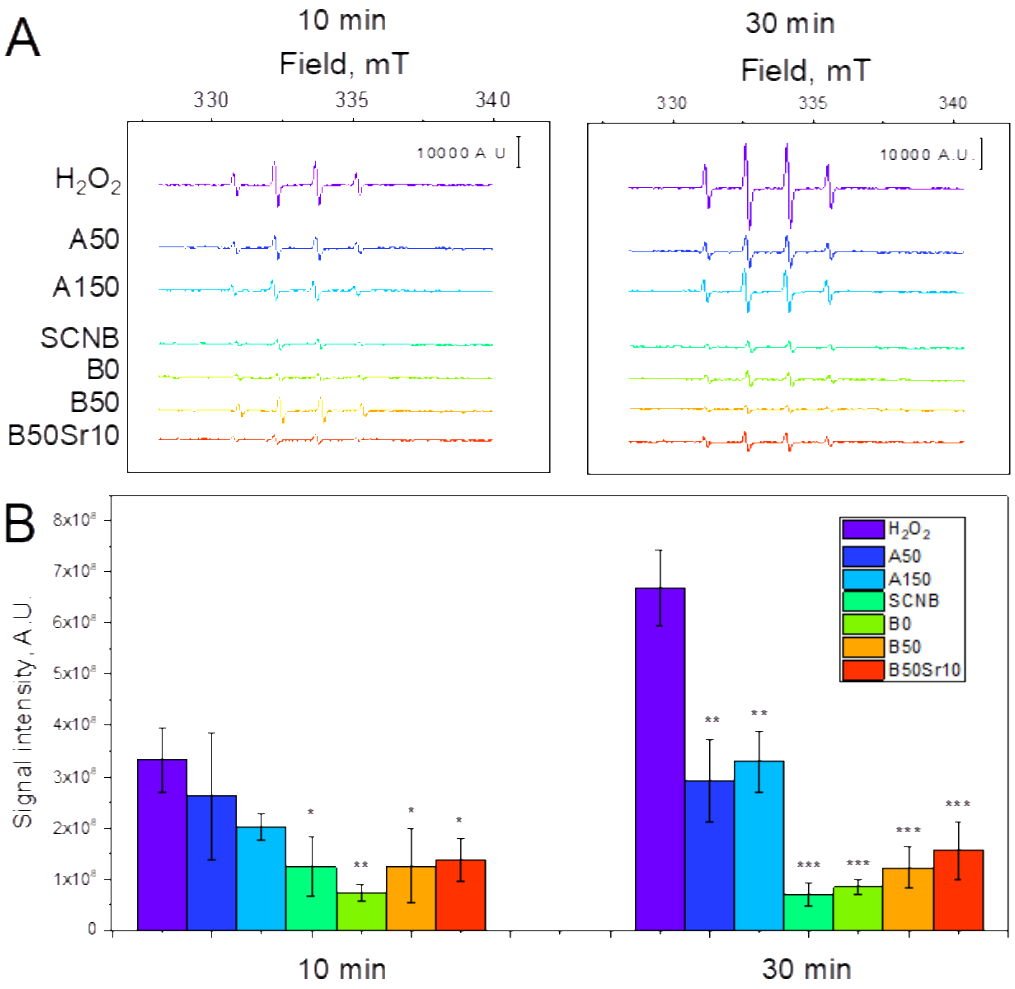


***Figure 10.*** *Radical scavenging activity measured by EPR-spin trapping at two different time of incubation. (A) Representative spectra of [DMPO-OH] and (B) [DMPO-OH] concentration obtained by double integration of EPR spectra of three different determinations. Data are reported as mean ± standard deviation of triplicate experiments. Columns that do not share at least one letter are statistically different (ANOVA, Tukey's test p <0.05).*

After 10 minutes of irradiation, the concentration of HO• detected with both the amorphous silica Aerosil 50 and Aerosil150 did not significantly differ from that detected in the ctrl+, indicating that at this time of incubation the effect of the mechanical annihilation of free radicals due to the impingement on the solid surface is not significant, even though a trend can be observed. All the tested bioactive glasses behave similarly and induced a significant decrease of HO• with respect to ctrl+. After 30 minutes of irradiation, the scavenging ability of the bioactive glasses becomes more evident both in comparison to ctrl+ and amorphous silica. Indeed, the concentration of HO• measured with all the bioactive glass samples was at least ca. 4-fold lower than that detected in the ctrl+. Moreover, all the bioactive glasses induced a significant higher, or at least the same, decrease of HO• concentration than the amorphous silica Aerosil50 and Aerosil150 did. Since the experiments were performed on a per mass basis, the exposed surface area of both the amorphous silica (i.e. 50 $m^2/g$ and 150 $m^2/g$ for Aerosil50 and Aerosil150, respectively) is considerably higher than that of the bioactive glass samples (3.3 $m^2/g$). This result highlights that the scavenging effect is not due a mere mechanical effect, but can be attributed to a specific chemical interaction of the bioactive glasses surface with photogenerated HO• radicals. Furthermore, with the glass powders the concentrations of HO• remained nearly constant at 10 and 30 minutes of irradiation evidencing that the glass antioxidant ability remains unvaried with the free radical increase.

On the basis of the contact angle, zeta potential and EPR results, a possible mechanism beyond this antioxidant capacity was hypothesized. Subsequently to the breakage of the structural units in the silica network, upon contact with the aqueous environment, the glass exposes –OH groups (Si-OH and/or B-OH) on its surface. It can be –OH act as preventive antioxidants (hydrogen donors) by yielding a hydrogen atom to the free radicals.

The negative charge of the resulted non-bridging oxygen (Si-O -) is compensated by the positive charge of the neighbor modifier cations (*e.g.*, $Ca^{2+}$ and $Na^{+}$), stabilizing the glass structure. Therefore, oxygen is unavailable for other reactions and the reactivity of the free radicals is extinguished, resulting in the interaction of the chain reactions at the base of the free radical production.

Considering these results, the mechanism beyond the radical scavenging ability of bioactive glasses, in absence of cells, seems strictly related to their hydroxylation ability and not to the release of specific ions, as previously observed by the authors for simple silicate bioactive glasses [19], and differently from specific antioxidant ions reported in the literature [13-17].

3.11 Biological evaluation

*3.11.1 Cytocompatibility*

Prior to test the potential antioxidant scavenger activity of the bioactive glasses, their cytocompatibility was assayed towards the human osteoblast progenitor cells hFOB. They represent a suitable *in vitro* model of cells deputed to the bone self-healing process as they were demonstrated to be able to differentiate towards a mature bone-like lineage without developing cells transformation [55]. So, hFOB cells were cultivated directly onto the specimens' surface and their metabolic activity as well as their morphology were compared to the same cells cultivated onto the gold standard polystyrene to rank the bioactive glasses cytocompatibility. Results are summarized in Figure 11.

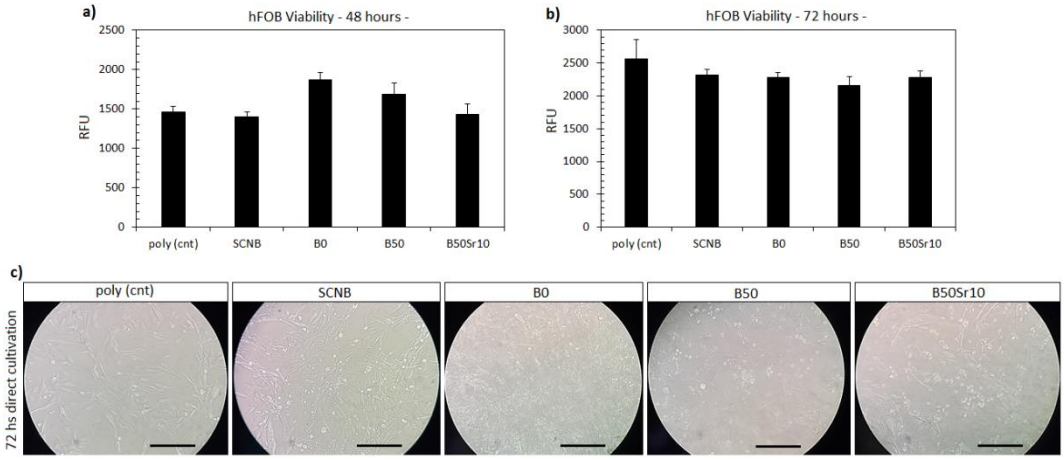


***Figure 11****. Cytocompatibility. All the test specimens resulted as cytocompatible towards hFOB cells as no significant differences (p>0.05) were noticed in terms of metabolic activity by comparing test bioactive glasses (SCNB, B0, B50, B50Sr10) with control polystyrene (poly cnt) at both 48 (a) or 72 (b) hour time-point.*

*Moreover, microscope images (c) showed that cells were adhered and spread in a comparable manner and density between test and control specimens. Bars represents means ± dev.st of 3 replicates; images bar scale = 100 $\mu$m.*

In general, the here developed innovative bioactive glasses (SCNB, B0, B50, B50sr10) resulted as highly compatible with hFOB cells as the observed metabolic activity was comparable with the polystyrene control at each 48 (Fig. 11 a) or 72 (Fig. 11 b) hour time-points ($p>0.05$). An early boost influencing cells metabolic activity was observed after 48 hours for B0, B50 and B50Sr10 specimens in comparison with polystyrene and SCNB; however, after 72 hours such effect was not observed anymore as all the values resulted as very similar to each other thus being time dependent. The effect can be ascribed to the different chemical composition of the tested bioactive glasses as some elements such as phosphorus and boron have been already shown to improve the viability and osteogenic differentiation of mesenchymal stem cells applied as model of tissue healing [56] without the need to introduce further biochemical stimulation such as alkaline phosphatase [57]. As a further demonstration of the bioactive glasses cytocompatibility, images of cells grown onto specimens' surface were collected after 72 hours cultivation (Fig. 11 c). Images showed that cells were able to adhere and spread onto test specimens' surface thus maintaining the typical fibroblast-like shape that is describe for these cells [58]. Some apoptotic round cells were observed too, but this can be ascribed to the neomycin enabling for the selection of resistant clones [58] as originally described by the Authors characterizing the hFOB cell line; in fact, the same effect was observed also in the polystyrene samples (poly cnt). So, the here developed bioactive glasses can be considered as ctyocompatible.

*3.11.2 Antioxidant scavenger activity*

After validating the bioactive glasses cytocompatibility towards human osteoblast progenitors, their ability of reducing oxidative stress by an intrinsic scavenger activity was evaluated in presence or absence of cells. Bulk values were collected in physiological conditions whereas the oxidative stress condition was induced by means of $H_2O_2$ addition into the medium within a daily routine (500 mM, 3 hours/day) previously

described by the Authors [19]. Then, the amount of oxygen and nitrogen active species (ROS/RNS) was evaluated as well as the potential protective activity of the bioactive glasses was assayed in relation to the cells' viability. Results of specimens tested without cells are summarized in Figure 12.

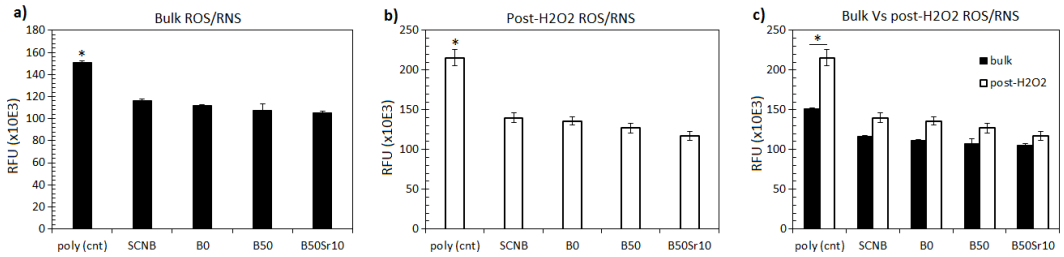


***Figure 12**. Scavenger activity without cells. Bioactive glasses demonstrated an intrinsic scavenger activity in reducing ROS/RNS amount both in physiological conditions (a) and after $H_2O_2$-induced oxidative stress (b) in comparison with polystyrene control. As a consequence, only polystyrene reported significant differences when bulk and post-$H_2O_2$ results were compared (c, indicated by *). Bars represent means ± dev.st of 3 replicates.*

Interesting, when ROS/RNS bulk values were evaluated in physiological conditions (i.e. in absence of induced oxidative stress), results obtained for cells cultivated into polystyrene were significantly higher than those obtained for the bioactive glasses (Fig. 12 a); so, an intrinsic anti-oxidant property seems to be outlined for the glasses. These data are in line to those recently published by the Authors showing that bioactive glasses in the simple silica-based composition were effective in protecting cells from oxidative stress thanks to a scavenger activity [19]. The presence of ROS/RNS species in physiological conditions is not surprising because unfortunately it represent a common condition for immortalized cells proliferating and replicating for many cycles; in fact, to preserve primary cells from oxidative stress due to culture conditions it has been demonstrated that the use of anti-oxidant chemicals can be of great benefit [59]. As demonstration of this theory, when oxidative stress was induced by $H_2O_2$ addition to improve the ROS/RNS level, polystyrene displayed once again significantly higher values than bioactive glasses (Fig. 12 b, $p<0.05$ indicated by *); therefore, the glasses were somehow able to counteract the active species increase. In fact,

when bulk and post-oxidative stress results were compared (Fig. 12 c), despite polystyrene started from the highest bulk values within all the groups, it was the only material showing a significant difference between the two conditions (Fig. 12 c, $p<0.05$ indicated by *). On the opposite, although an increase of ROS/RNS level was found, bioactive glasses did not report significant differences by comparing physiological and stressed conditions, therefore confirming a strong ability to scavenge active species.

Afterwards, the same conditions were repeated after cultivating cells for 72 hours onto specimens and polystyrene surfaces. In this experimental condition, the cells' viability was selected as target to test bioactive glasses ability to protect cells from toxic active species due to their scavenger ability. Results are summarized in Figure 13.

In general, results are in line to those obtained for the ROS/RNS evaluation. In the bulk condition (Fig. 13 a), no differences ($p>0.05$) were reported as previously showed for the cytocompatibility assay; however, when oxidative stress condition was induced the viability of cells after 3 days was significantly higher in B0, B50 and B50Sr10 is compared to polystyrene control (Fig. 13 b, $p<0.05$ indicated by §). So, it can be speculated that the bioactive glasses are capable of scavenge most of the toxic active species released in the medium due to the $H_2O_2$ addition, thus preserving cells from apoptosis. As previously hypothesized by the Authors [19], this effect can depend by the glasses' composition because the presence of -OH groups exposed to the surface can be effective in binding the generated RONS that are not free to affect cells growing onto specimens' surface. On the opposite, polystyrene control lacks such protective mechanism thus being nor able to protect cells from oxidative stress-induced apoptosis.

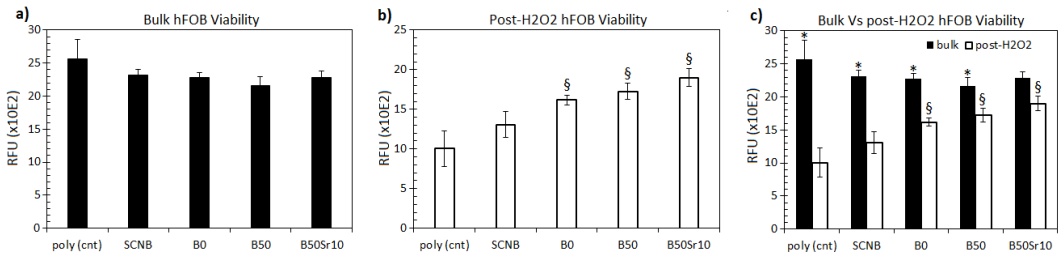


***Figure 13**. Scavenger activity in presence of cells. Bioactive glasses demonstrated to be cytocompatible (a) and to hold an intrinsic scavenger activity in reducing ROS/RNS amount that protected cells toxic species. In*

*fact, cells viability was significantly higher in B0, B50 and B50Sr10 than polystyrene (b, p<0.05 indicated by §) as well as for B50Sr10 there was no significant difference between bulk and post-$H_2O_2$ treatment (c). Bars represent means ± dev.st of 3 replicates.*

Finally, bulk and post-$H_2O_2$ treatment results were compared (Fig. 13 c). Here, only the B50Sr10 glasses did not report significant differences between the two groups, thus showing the best protective effect towards cells cultivated in stressing condition. Differently, all the other bioactive glasses reported a significant release of cells' viability after $H_2O_2$ treatment ($p<0.05$, indicated by *) even if the values were in general 60-80% higher than polystyrene thus confirming a protective effect. In presence of cells a more evident difference between the glass formulations emerges evidencing the role of specific ions (such as Sr), in addition to the hydroxylation degree, in the antioxidant ability of bioactive glasses.

**4. Conclusions**

In the present work, four silicate and borosilicate bioactive glasses have been synthetized and characterized for their surface properties (wettability, charge, hydroxylation degree, reactivity in SBF and Tris buffer) and antioxidant activity, in presence and absence of osteoblast cells, in order to understand the mechanisms of the intrinsic antioxidant ability of bioactive glasses.

The results obtained on bulk samples concerning molar volume, pH, ion release and FTIR spectroscopy, before and after immersion in buffered solutions, have proved to be coherent showing what follows. The positive effect of boron in enhancing the glass reactivity (B50 bulk samples data), leading to an increase of both dissolution rate and formation of an HCA layer on the glass surface. The stabilizing role of Sr and Mg, resulting in a lower dissolution rate and in a reduced precipitation of HCA on the surface (B50Sr10 bulk samples data), which can be explained by the presence in the glass network of three different alkaline earth elements (Ca, Mg, Sr) with different atomic radius sizes: different atomic radii allow to occupy a larger number of interstices in the glass network. The difference between Tris and SBF buffers (bulk samples data), due to the presence of ions in the solution, besides those released from the glass surface: SBF

contains a significant amount of Ca and P, and tends to saturate faster by forming a thicker HCA layer, whereas the lack of ions in Tris leads to a more sustained glass dissolution and to a delayed layer formation. As concerning the antioxidant ability, from the outcomes of the EPR experiment the scavenging potential of the four analyzed bioactive glasses towards reactive oxygen species (ROS) was clearly proved. The more remarkable data is their ability of maintaining the OH • levels constant with time, despite the increase production of free radicals in the solution. The hypothesis assuming –OH groups as possible hydrogen donors seems confirmed, but further investigations are still needed to definitively demonstrate this process, since it is not easy to measure the precise amount of –OH on the glass surface in relation with the other component of the silica network. Results of cellular test confirm once again the protective effect of bioactive glasses toward ROS/RNS species. Indeed, cells' metabolic activity was preserved when seeded onto BG specimens, whereas a significant reduction was observed for cells cultivated onto polystyrene surface. The higher antioxidant activity of B50Sr10 confirm the possibility of strontium in stimulating the activation of natural cell antioxidant defenses. Cellular test results give also evidence of the benefit role of boron in enhancing the natural antioxidant defense system in cells, as reported in previous study. In conclusion, in this work, the characterization of our samples has proved the biocompatibility and bioactivity of SCN, B0, B50 and B50Sr10 bioactive glasses, showing additionally some properties proposed previously in other studies. But more important, we gave a clearly demonstration of the presence of an antioxidant capacity in not-doped bioactive glasses, remaining constant during time, and for the first time a hypothesis has been made about the mechanism beyond this antioxidant capacity.

**Acknowledgements**

This work was self-funded thanks to the Assignments for Basic Research (2017-2020) provided by Politecnico di Torino. The authors would like to acknowledge the Tampere Microscopy Center (especially Turkka Salminen) for providing the Raman spectra.

**References**

[1] J. R. Jones, Review of bioactive glass: From Hench to hybrids, Acta Biomater. 9(1) (2013) 4457–4486. https://doi: 10.1016/j.actbio.2012.08.023

[2] J.M. Oliveira, R.N. Correia, M.H. Fernandes, Effect of Si speciation on the in vitro bioactivity of glasses, Biomaterials 23 (2002) 371-379. https://doi.org/10.1016/S0142-9612(01)00115-6

[3] L.L. Hench, Bioceramics, J. Am. Ceram. Soc. 81(7) (1998) 1705-28. https://doi.org/10.1111/j.1151-2916.1998.tb02540.x

[4] H. Kim, F Miyaji, T. Kokubo, Bioactivity of $Na_2O$-CaO-$SiO_2$ Glasses, J. Am. Ceram. Soc. 79(9) (1995) 2405-11. https://doi.org/10.1111/j.1151-2916.1995.tb08677.x

[5] S. Ferraris , A. Nommeot-Nomm , S. Spriano , E. Vernè , J. Massera, Surface reactivity and silanization ability of borosilicate and Mg-Sr-based bioactive glasses, Applied Surface Science, 475(2019) 43-55. http://dx.doi.org/10.1016/j.apsusc.2018.12.218

[6] Q. Fu, M.N. Rahaman, B.S. Bal, L.F. Bonewald, K. Kuroki, R.F. Brown, Silicate, borosilicate, and borate bioactive glass scaffolds with controllable degradation rate for bone tissue engineering applications. II. In vitro and in vivo biological evaluation. J Biomed Mater Res A. 95(1) (2010) 172-9. doi: 10.1002/jbm.a.32823. PMID: 20540099.

[7] M. Ojansivu, A. Mishra, S. Vanhatupa, M. Juntunen, A. Larionova, J. Massera, et al., The effect of S53P4-based borosilicate glasses and glass dissolution products on the osteogenic commitment of human adipose stem cells. PLoS ONE 13(8) (2018) e0202740. https://doi.org/10.1371/ journal. pone.0202740

[8] W. Huang, D.E. Day, K. Kittiratanapiboon, M.N. Rahaman, Kinetics and mechanisms of the conversion of silicate (45S5), borate, and borosilicate glasses to hydroxyapatite in dilute phosphate solutions, J Mater Sci: Mater Med, 17 (2006) 583-596. https://doi.org/10.1007/s10856-006-9220-z

[9] A. Hoppe, N. S. Güldal, A. R. Boccaccini, A review of the biological response to ionic dissolution products from bioactive glasses and glass-ceramics, Biomaterials 32 (2011) 2757-2774. https://doi.org/10.1016/j.biomaterials.2011.01.004

[10] F. Rosenfeldt, M. Wilson, G. Lee, C. Kure, R. Ou, L. Braun, J. de Haan, Oxidative stress in surgery in an ageing population: pathophysiology and therapy, Experimental Gerontology 48 (2013) 45-54. https://doi.org/10.1016/j.exger.2012.03.010

[11] M. Abdollahi, B. Larijani, R. Rahimi, P. Salari, Role of oxidative stress in osteoporosis, Therapy 2 (2005) 787-796. DOI:10.1586/14750708.2.5.787

[12] Miola M., Vitale Brovarone C., Maina G., Rossi F., Bergandi L., Ghigo D., Saracino S., Maggiora M., Canuto R.A., Muzio G., Vernè E. In vitro study of manganese-doped bioactive glasses for bone regeneration. Materials Science and Engineering C, 38 (1)(2014) 107-118. ISSN: 0928-4931; DOI: 10.1016/j.msec.2014.01.045

[13] V. Nicolini, E. Gambuzzi, G. Malavasi, L. Menabue, MC menziani, G. lusvardi, A. Pedone, F. Benedetti, P. luches, S. D'Addato, S. Valeri, Evidence of catalase mimetic activity in Ce3+/ce4+ doped bioactive glasses, J Phys Chem B 119 (2015) 4009-4019. https://doi.org/10.1021/acs.jpcb.7b05993

[14] A. Pedone, F. Muniz-Miranda, A. Tilocca, M.C. Menziani. The antioxidant properties of Ce-containing bioactive glass nanoparticles explained by molecular dynamics simulations, Biomed Glasses 2 (2016) 19-28. DOI: 10.1515/bglass-2016-0003

[15] S. Jebahi, H. Oudadesse, H. el Feki, T. Rebai, H. Keskes, P. Pellen, A. el Feki, Antioxidant/oxidative effects of strontium doped bioactive glass as bone graft. In vivo assay in ovariectomized rats, J. Appl. Biomed 10 (2012) 195-209. DOI: 10.2478/v10136-012-0009-8

[16] S. Kapoor, A. Goel, A. Tilocca, V. Dhuna, G. Bhatia, K. Dhuna, JMF Ferreira, Role of glass structure in defining the chemical dissolution behavior, bioactivity and antioxidant properties of zinc and strontium co-doped alkali-free phosphosilicate glasses, Acta Biomaterialia 10 (2014) 3264-3278. https://doi.org/10.1016/j.actbio.2014.03.033

[17] M. Miola, J. Massera, A. Cochis, A. Kumar, L. Rimondini, E. Vernè, Tellurium: A new active element for innovative multifunctional bioactive glasses, Materials Science & Engineering C 123 (2021) 111957. https://doi.org/10.1016/j.msec.2021.111957

[18] M. Cazzola, I. Corazzari, E. Prenesti, E. Bertone, E. Vernè, S. Ferraris, Bioactive glass coupling with natural polyphenols: Surface modification, bioactivity and anti-oxidant ability, Applied Surface Science 367 (2016) 237–248. https://doi.org/10.1016/j.apsusc.2016.01.138

[19] S. Ferraris, I. Corazzari, F. Turci, A. Cochis, L. Rimondini, E. Vernè, Antioxidant activity of silica based bioactive glasses, ACS Biomater. Sci. Eng. 7 (2021) 2309−2316. doi: 10.1021/acsbiomaterials.1c00048

[20] T. Kokubo, H. Takadama, How useful is SBF in predicting in vivo bone bioactivity? Biomaterials, 27 (2006), 2907-2915. https://doi.org/10.1016/j.biomaterials.2006.01.017

[21] T. Kokubo, H. Kushitani, S. Sakka, T. Kitsugi, T. Yamamuro, Solutions able to reproduce in vivo surface-structure changes in bioactive glass-ceramics A-W, Journal of Biomedical Materials Research, 24 (1990)721-734. https://doi.org/10.1002/jbm.820240607

[22] X. Hou, R.S. Amais, B.T.Jones, G.L. Donati, Inductively Coupled Plasma Optical Emission Spectrometry, Encyclopedia of Analytical Chemestry, (2016) 1-25. https://doi.org/10.1002/9780470027318.a5110.pub3

[23] T. Luxbacher, The ZETA Guide Principles of the Streaming Potential Technique, Anton Paar, 2014.

[24] D.S. Brauer, Bioactive Glasses—Structure and Properties, Angew. Chem. Int. Ed., 54 (2015)4160–4181. https://doi.org/10.1002/anie.201405310

[25] M. Tylkowski, D.S.,Brauer, Mixed alkali effects in Bioglass® 45S5, Journal of Non-Crystalline Solids, 376 (2013)175-181. https://doi.org/10.1016/j.jnoncrysol.2013.05.039

[26] I. Elgayar, Aliev, A.E., A.R. Boccaccini, R.G. Hill, Structural analysis of bioactive glasses, Journal of Non-Crystalline Solids, 351 (2005)173-183. https://doi.org/10.1016/j.jnoncrysol.2004.07.067

[27] J. Massera, L. Hupa, Influence of SrO substitution for CaO on the properties of bioactive glass S53P4. *J Mater Sci: Mater Med* **25,** 657–668 (2014). https://doi.org/10.1007/s10856-013-5120-1

[28] S. Ferraris, A. Nommeots-Nomm, S. Spriano, E. Vernè, J. Massera, Surface reactivity and silanization ability of borosilicate and Mg-Sr-based bioactive glasses, Applied Surface Science, 475(2019) 43-55. http://dx.doi.org/10.1016/j.apsusc.2018.12.218

[29] J.M. Tainio, D.A.A. Salazar, A. Nommeots-Nomm, C. Roiland, B.Bureau, D.R. Neuville, D.S. Brauer, & J.Massera, Structure and in vitro dissolution of Mg and Sr containing borosilicate bioactive glasses for bone tissue engineering, Journal of Non-Crystalline Solids, 533(2020)119893. https://doi.org/10.1016/j.jnoncrysol.2020.119893

[30] L. Marsich, L. Moimas, V. Sergo, C. Schmid, Raman spectroscopy study of bioactive silica-based glasses: The role of the alkali/alkali earth ratio on the Non-Bridging Oxygen/Bridging Oxygen (NBO/BO) ratio, Spectroscopy, 23 (2009) 227-232. https://doi.org/10.3233/SPE-2009-0380

[31] D. Manara, A. Grandjean, D.R. Neuville, Advances in understanding the structure of borosilicate glasses: A Raman spectroscopy study, American Mineralogist, 94 (2009) 777-784. https://doi.org/10.2138/am.2009.3027

[32] M. Bohner, J. Lemaitre, Can bioactivity be tested in vitro with SBF solution? Biomaterials, 30(12)(2009)2175-9. doi: 10.1016/j.biomaterials.2009.01.008. Epub 2009 Jan 26

[33] K. Schuhladen, X. Wang, L. Hupa, A. R. Boccaccini, Dissolution of borate and borosilicate bioactive glasses and the influence of ion (Zn, Cu) doping in different solutions, Journal of Non-Crystalline Solids, 502(2018)22-34. https://doi.org/10.1016/j.jnoncrysol.2018.08.037

[34] Y. C. Fredholm, N. Karpukhina, D. S. Brauer, J. R. Jones, R. V. Lawand, R. G. Hill, Influence of strontium for calcium substitution in bioactive glasses on degradation, ion release and apatite formation, R. Soc. Interface, 9 (2012) 880–889. https://doi.org/10.1098/rsif.2011.0387

[35] L. Varila, S. Fagerlund, T. Lehtonen, J. Tuominen, L. Hupa, Surface reactions of bioactive glasses in buffered solutions, Journal of the European Ceramic Society, 32 (2012) 2757-2763. https://doi.org/10.1016/j.jeurceramsoc.2012.01.025

[36] M. Mneimne, R.G. Hill, A.J. Bushby, D.S. Brauer, High phosphate content significantly increases apatite formation of fluoride containing bioactive glasses, Acta Biomaterialia, 7 (2011)1827-1834. https://doi.org/10.1016/j.actbio.2010.11.037

[37] M.G. Cerutti, D. Greenspan, K. Powers, An analytical model for the dissolution of different particle size samples of Bioglass® in Trisbuffered solution, Biomaterials, Vol. 26 (2005), pp. 4903-4911. https://doi.org/10.1016/j.biomaterials.2005.01.013

[38] Serra J, González P, Liste S, Serra C, Chiussi S, León B, Pérez-Amor M, Ylänen HO, Hupa M. FTIR and XPS studies of bioactive silica-based glasses. J Non-Cryst Solids. 332(2003) 20–7. https://doi.org/10.1016/j.jnoncrysol.2003.09.013

[39] L. Stoch, M. Środa, Infrared spectroscopy in the investigation of oxide glasses structure. J Mol Struct. 511–512 (1999)77–84. https://doi.org/10.1016/S0022-2860(99)00146-5

[40] M. Szumera, I. Waclawska, Z. Olenjniczak, Influence of $B_2O_3$ on the structure and crystallization of soil active glasses. J Therm Anal Calorim. 99 (2010)879–86. https://doi.org/10.1007/s10973-009-0550-1

[41] G.J. Bentrup, H.M.M. Moawad, L.F. Santos, R.M. Almeida, H. Jain, Structure of $Na_2O–CaO–P_2O_5–SiO_2$ glass–ceramics with multimodal porosity. J Am Ceram Soc.92(2009)249–52. https://doi.org/10.1111/j.1551-2916.2008.02847.x

[42] A.C. Queiroz, J.D. Santos, F.J. Monteiro, M.H. Prado da Silva. Dissolution studies of hydroxyapatite and glass-reinforced hydroxyapatite ceramics. Mater Charact. 50(2003)197–202. https://doi.org/10.1016/S1044-5803(03)00092-5

[43] P. Pascuta, M. Bosca, S. Rada, M. Culea, I. Bratu, E. Culea, FTIR Spectroscopic Study of $Gd_2O_3$-$Bi_2O_3$-$B_2O_3$ Glasses, Journal of Optoelectronics and Advanced Materials, 10 (2008) 2416-2419. https://doi.org/10.1016/S1044-5803(03)00092-5

[44] L. Koudelka, P. Mosner, Borophosphate Glasses of the ZnO-$B_2O_3$-$P_2O_5$ System, Materials Letters, 42 (2000) 194. https://doi.org/10.1016/S0167-577X(99)00183-4

[45] C. Gautam, A.K. Yadav, A.K. Singh, A Review on Infrared Spectroscopy of Borate Glasses with Effects of Different Additives, International Scholarly Research Network, 2012 (2012) 1-17. https://doi.org/10.5402/2012/428497

[46] J. Massera, L.Hupa, Influence of SrO substitution for CaO on the properties of bioactive glass S53P4. J Mater Sci: Mater Med **25,** 657–668 (2014). https://doi.org/10.1007/s10856-013-5120-1

[47] M Ojansivu, A Mishra, S Vanhatupa, M Juntunen, A Larionova, J Massera, S. Miettinen, The effect of S53P4-based borosilicate glasses and glass dissolution products on the osteogenic commitment of human adipose stem cells. PLoS ONE 13 (2018) e0202740. https://doi.org/10.1371/ journal.pone.0202740

[48] S. Di Nunzio, C. Vitale Brovarone, S. Spriano, D. Milanese, E. Verne´, V. Bergo, G. Maina, P. Spinelli, Silver containing bioactive glasses prepared by molten salt ion-exchange, Journal of the European Ceramic Society 24 (2004) 2935–2942

[49] F.C. Celikenzen, H. Turkez, E. Aydin, M.S. Izgi, B. Celikezen, Potent antioxidant and genotoxic effects of ammonium tetra borate in vitro, Natural Science and Discovery, 1 (2015), 45-49. https://doi.org/10.20863/nsd.v1i2.7

[50] T.V. Bhasker, N.K. Gowda, S. Mondal, Krishnamoorthy, P., Pal, D.T., Mor, A., Bhat, S.K., Pattanaik, A.K., Boron influences immune and antioxidant responses by modulating hepatic superoxide dismutase activity

under calcium deficit abiotic stress in Wistar rats; Journal of Trace Elements in Medicine and Biology, Vol. 36 (2016), pp. 73-79. https://doi.org/10.1016/j.jtemb.2016.04.007

[51] G. Berlier, L. Gastaldi, S. Sapino, I. Miletto, E. Bottinelli, D. Chirio, E. Ugazio, MCM-41 as a useful vector for rutin topical formulations: synthesis, characterization and testing, Int. J. Pharm. 457 (2013) 177–186. DOI: 10.1016/j.ijpharm.2013.09.018

[52] http://www.xpsfitting.com/2011/03/c-1s-carbonates.html (accessed 5th April 2022).

[53] J. Serra, P. Gonzalez , S. Liste , C. Serra , S. Chiussi , B. Leon, M. Perez-Amor, H.O. Ylanen , M. Hupa, FTIR and XPS studies of bioactive silica based glasses, Journal of Non-Crystalline Solids 332 (2003) 20–27. https://doi.org/10.1016/j.jnoncrysol.2003.09.013

[54] E. Verne´, C. Vitale-Brovarone, E. Bui, C. L. Bianchi, A. R. Boccaccini, Surface functionalization of bioactive glasses, Inc. J Biomed Mater Res 90A(2009) 981–992. https://doi.org/10.1002/jbm.a.32153

[55] M. Subramaniam, S. M. Jalal, D. J. Rickard, S. A. Harris, M. E. Bolander, T. C. Spelsberg, Further characterization of human fetal osteoblastic hFOB 1.19 and hFOB/ERα cells: Bone formation in vivo and karyotype analysis using multicolor fluorescent in situ hybridization. Journal of cellular biochemistry, 87(1) (2002) 9-15. https://doi.org/10.1002/jcb.10259

[56] K. C. Feng, Y. J. Wu, C. Y. Wang, C. S.,Tu, Y. L. Lin, C. S. Chen, P.L. Lai, I.T. Huang, P. Y. Chen, Enhanced mechanical and biological performances of CaO-MgO-$SiO_2$ glass-ceramics via the modulation of glass and ceramic phases. Materials Science and Engineering: C, 124 (2021) 112060. https://doi.org/10.1016/j.msec.2021.112060

[57] E. Vernè, S. Ferraris, C. Vitale-Brovarone, A. Cochis, L. Rimondini, Bioactive glass functionalized with alkaline phosphatase stimulates bone extracellular matrix deposition and calcification in vitro. Applied surface science, 313 (2014) 372-381. https://doi.org/10.1016/j.apsusc.2014.06.001

[58] S. A. Harris, R. J. Enger, L. B. Riggs, T. C. Spelsberg, Development and characterization of a conditionally immortalized human fetal osteoblastic cell line. Journal of Bone and Mineral Research, 10(2) (1995) 178-186. https://doi.org/10.1002/jbmr.5650100203

[59] N. Suh & E. B. Lee, Antioxidant effects of selenocysteine on replicative senescence in human adipose-derived mesenchymal stem cells. BMB reports, 50(11) (2017) 572. https://doi.org/10.5483/BMBRep.2017.50.11.174